Contributions to Mineralogy and Petrology (2018) 173:11
https://doi.org/10.1007/s00410-017-1437-y

ORIGINAL PAPER

Origins and evolution of rhyolitic magmas in the central Snake River Plain: insights from coupled high-precision geochronology, oxygen isotope, and hafnium isotope analyses of zircon

Dylan P. Colón[1] · Ilya N. Bindeman[1] · Jörn-Frederik Wotzlaw[2] · Eric H. Christiansen[3] · Richard A. Stern[4]

Received: 25 May 2017 / Accepted: 26 December 2017 / Published online: 13 January 2018

Abstract

We present new high-precision CA-ID-TIMS and in situ U–Pb ages together with Hf and O isotopic analyses (analyses performed all on the same grains) from four tuffs from the 15−10 Ma Bruneau–Jarbidge center of the Snake River Plain and from three rhyolitic units from the Kimberly borehole in the neighboring 10−6 Ma Twin Falls volcanic center. We find significant intrasample diversity in zircon ages (ranges of up to 3 Myr) and in $\delta^{18}O$ (ranges of up to 6‰) and ε_{Hf} (ranges of up to 24 ε units) values. Zircon rims are also more homogeneous than the associated cores, and we show that zircon rim growth occurs faster than the resolution of in situ dating techniques. CA-ID-TIMS dating of a subset of zircon grains from the Twin Falls samples reveals complex crystallization histories spanning 10^4–10^6 years prior to some eruptions, suggesting that magma genesis was characterized by the cyclic remelting of buried volcanic rocks and intrusions associated with previous magmatic episodes. Age-dependent trends in zircon isotopic compositions show that rhyolite production in the Yellowstone hotspot track is driven by the mixing of mantle-derived melts (normal $\delta^{18}O$ and ε_{Hf}) and a combination of Precambrian basement rock (normal $\delta^{18}O$ and ε_{Hf} down to −60) and shallow Mesozoic and Cenozoic age rocks, some of which are hydrothermally altered (to low $\delta^{18}O$ values) by earlier stages of Snake River Plain magmatism. These crustal melts hybridize with juvenile basalts and rhyolites to produce the erupted rhyolites. We also observe that the Precambrian basement rock is only an important component in the erupted magmas in the first eruption at each caldera center, suggesting that the accumulation of new intrusions quickly builds an upper crustal intrusive body which is isolated from the Precambrian basement and evolves towards more isotopically juvenile and lower-$\delta^{18}O$ compositions over time.

Keywords Snake river plain · Zircon · Rhyolite · Geochronology · Oxygen isotopes · Hafnium isotopes

Introduction

The Columbia River Basalt–Snake River Plain–Yellowstone system is the world's premiere example of a continental hotspot track (Fig. 1). It is the site of many of the most voluminous volcanic eruptions in the Neogene Period (Christiansen 2001; Hildreth et al. 1991; Pierce and Morgan 2009), and comprises one of the largest suites of anorogenic (A-type) rhyolites worldwide (Christiansen and McCurry 2008; Pearce et al. 1984). The Yellowstone hotspot track additionally includes the largest known concentration of low-$\delta^{18}O$ rhyolites in the world, with a cumulative volume of over 10^4 km^3 (Bonnichsen et al. 2008; Bindeman and Simakin 2014). Low $\delta^{18}O$ values in fresh igneous rocks were once considered to be geologic oddities (e.g. Hildreth et al. 1984), but they have since been found around the world, particularly in association with extensional tectonics and large

Communicated by Gordon Moore.

Electronic supplementary material The online version of this article (doi:https://doi.org/10.1007/s00410-017-1437-y) contains supplementary material, which is available to authorized users.

✉ Dylan P. Colón
dcolon@uoregon.edu

[1] University of Oregon, Eugene, OR, USA

[2] Department of Earth Sciences, Institute of Geochemistry and Petrology, ETH Zürich, Zurich, Switzerland

[3] Brigham Young University, Provo, UT, USA

[4] University of Alberta, Edmonton, AB, Canada

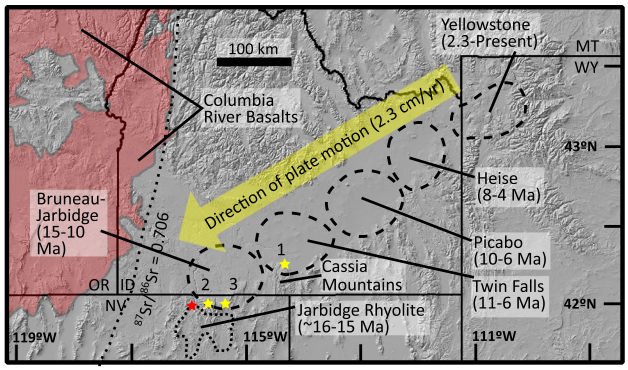

Fig. 1 Map of the Yellowstone hotspot track, showing the major volcanic centers that formed after the onset of the eruption of the Columbia River Flood Basalts (red). Three yellow stars are sampling locations for this study: (1) the Kimberly borehole, (2) along the Bruneau River, and (3) along the Jarbidge River. The red star is the site of the J-P Desert locality discussed in the text and in Colón et al. (2015b). Outlines of volcanic centers are from Bonnichsen et al. (2008) and Colón et al. (2015b). Plate velocity is from Anders et al. (2014). Map background is from Ryan et al. (2009) via GeoMapApp (http://www.geomappapp.org/)

igneous provinces (both present at Yellowstone). Examples include rhyolites and basalts in Iceland (Gautason and Muehlenbachs 1998; Bindeman et al. 2012; Zierenberg et al. 2013), Archean extensional granites in Greenland (Hiess et al. 2011), rhyolites in the Karoo Volcanic Province in Africa and Antarctica (Harris and Erlank 1992), younger rifted-margin granites in South Africa (Curtis et al. 2013), Jurassic granites of the North China Craton (Wang et al. 2017a), Proterozoic granites of east-central and south China, Seychelles, and Madagascar (Archibald et al. 2016; Fu et al. 2013; Harris and Ashwal 2002; Zheng et al. 2007), and rhyolites of the Proterozoic Malani Igneous Suite in India (Wang et al. 2017b).

The Snake River Plain–Yellowstone system is the youngest and likely the best-preserved of these suites globally, making it the ideal laboratory for the detailed study of the origin of these types of magmas worldwide. In this study, we make measurements of the O and Hf isotopic compositions of zircon grains from central Snake River Plain rhyolites and combine them with precise U–Pb ages of those same crystals. The relative youth of Snake River Plain volcanism compared to many other low-$\delta^{18}O$ anorogenic igneous suites allows us to make detailed measurements of the time-dependent changes in both O and Hf isotope compositions of its magmas, and recently developed high-precision dating techniques allow us to study variations in the ages of zircon from a single eruption (e.g. Rivera et al. 2016; Wotzlaw et al. 2013, 2014, 2015). Finally, we combine our results with data from several other recent studies of Yellowstone hotspot track O and Hf isotopes in zircon to identify isotopic trends common to the entire hotspot track, as opposed to those dependent on local geology, allowing us to determine which processes may be properties of similar igneous suites around the world.

Geologic setting

Previous work on Yellowstone hotspot zircon has identified considerable isotopic diversity (Fig. 9) which has been interpreted as the result of variable mixing between a mantle-like end-member ($\delta^{18}O \approx +5.7‰$ VSMOW; $\varepsilon_{Hf} = 0$ to $+5$) considered to be isotopically identical to basalts from the Snake River Plain/Yellowstone (e.g. Stelten et al. 2017) and up to 60% of some combination of end-member crustal compositions (Colón et al. 2015b; Drew et al. 2013; Wotzlaw et al. 2015). These crustal end-members are visible in Fig. 9, which combines previous measurements of Hf and O isotopes along the hotspot track with data from this study. We intentionally leave out rhyolites from west of the $^{87}Sr/^{86}Sr = 0.706$ line (Fig. 1) which defines the edge of the Precambrian core of North America (Leeman 1992; Nash et al. 2006), as these rhyolites were produced in significantly different crust and with very different rates of basaltic intrusion from the mantle (Blum et al. 2016; Coble and Mahood 2012; Ferns and McClaughry 2013; Colón et al. 2015a). The first crustal end-member has been interpreted as ancient Proterozoic or even Archean crust with exceptionally unradiogenic (low-ε_{Hf}) hafnium isotopic compositions, and relatively normal $\delta^{18}O$ values (+5–8‰); xenoliths of such material have been observed throughout the Snake River Plain, despite the relative paucity of surface outcrops (Leeman et al. 1985; Watts et al. 2010; Shirley 2013). The unit on the hotspot track containing the most of this end-member is the Jarbidge Rhyolite (Colón et al. 2015b), which has zircon with ε_{Hf} values as low as − 39, the lowest value observed in a non-xenocrystic zircon in the entire region (Fig. 9).

The second crust type is very low-$\delta^{18}O$ and only moderately unradiogenic in terms of Hf isotopes, and is well-represented among Snake River Plain and Yellowstone zircon grains (Fig. 9). This material must have been hydrothermally altered in the presence of meteoric water, and has previously been proposed to be (1) deeply buried and syn-volcanically altered caldera-filling ignimbrites, (Bindeman and Valley 2001; Colón et al. 2015b; Drew et al. 2013; Watts et al. 2011), (2) shallow crustal rocks that were hydrothermally altered during some magmatic event that significantly predates Yellowstone volcanism, such as the emplacement of the Idaho and Challis batholiths (Boroughs et al. 2012; Ellis et al. 2013; Drew et al. 2013), or (3) shallow country rocks or juvenile (Yellowstone hotspot-age) intrusions altered by hydrothermal circulation driven by heat produced by intrusions of basalt coeval with the Columbia River Basalts and early Snake River Plain volcanism (Blum et al. 2016; Colón

et al. 2015a, b). The first explanation is inadequate on its own at the central Snake River Plain (Bruneau–Jarbidge and Twin Falls, Fig. 1) because the erupted rhyolites there are exclusively low-$\delta^{18}O$ (Colón et al. 2015b), uniquely among the rhyolitic centers of the region (Bindeman and Simakin 2014), precluding a role for buried young ignimbrites from the same system in the production of the first low-$\delta^{18}O$ eruptions. The earliest low-$\delta^{18}O$ rhyolites of the central Snake River Plain are thus likely derived from some combination of the latter two mechanisms, with a possible role for caldera burial in producing the later, even lower-$\delta^{18}O$ rhyolites (Colón et al. 2015b). We note that the second two options assume the hydrothermal alteration of some pre-existing crust, but option (3) assumes that this happened only shortly before rhyolite production, and includes juvenile intrusions with older crust in the collection of material that is hydrothermally altered.

To date, only limited work on zircon isotope geochemistry has been published for the Bruneau–Jarbidge and Twin Falls centers (Cathey et al. 2011; Seligman 2012; Couper 2016; Blum et al. 2016; Fig. 1), even though they are both the most voluminous and the only exclusively low-$\delta^{18}O$ rhyolitic centers on the entire hotspot track (Bonnichsen et al. 2008; Ellis et al. 2013). This fact makes their study critical to any broader investigation of the origins of low-$\delta^{18}O$ magmas at Yellowstone, and any extrapolation to other volcanic provinces worldwide. In this study, we measured coupled O and Hf isotope compositions of zircon grains from four large-volume ignimbrites from the Bruneau–Jarbidge center and from three units from the Twin Falls center, filling in this crucial gap. This data is complemented by laser ablation U–Pb geochronology and further dating via chemical abrasion isotope dilution thermal ionization mass spectrometry (CA-ID-TIMS) performed on the same crystals after removing them from the mounts used for spot analyses. These techniques provide new insights into the volcanic centers of the central Snake River Plain, building on earlier petrologic work by Cathey and Nash (2004) and Ellis and Wolff (2012).

Sampling of Bruneau–Jarbidge and Twin Falls rhyolites

At the Bruneau–Jarbidge center, we collected one sample each from four large welded ignimbrite outflow sheets. At a locality along the southern Jarbidge River in Nevada, we collected the 11.81 ± 0.06 Ma Cougar Point Tuff (CPT) VII and the 10.79 ± 0.14 Ma CPT XIII ($^{40}Ar/^{39}Ar$ ages of Bonnichsen et al. 2008; Fig. 1). The other two units were collected at the Bruneau River Canyon, approximately 20 km west of the first site, and are the 12.07 ± 0.08 Ma CPT V ($^{40}Ar/^{39}Ar$ age of Perkins et al. 1998) and a previously unnamed tuff unit at the base of the section. The latter unit predates CPT III, the previously oldest described member of the Cougar Point Tuff sequence, and we will refer to it as the tuff of Bruneau Canyon, though a name of Cougar Point Tuff I or Cougar Point Tuff II (no existing units have these names) may eventually prove to be more appropriate (Bonnichsen and Citron 1982). These samples were chosen to encompass both the early and late stages of the eruptive sequence.

At the younger Twin Falls center (Figs. 1, 2), we sampled the three rhyolitic units intersected by the Kimberly borehole of Project Hotspot (Knott et al. 2016; Shervais et al. 2014). The uppermost of these is the Shoshone Rhyolite, dated by Knott et al. (2016) by single-grain laser fusion $^{40}Ar/^{39}Ar$ at 6.37 ± 0.44 Ma using plagioclase. This unit is buried by about 100 m of young basalt flows, and is itself just over 100 m thick. It appears to be a lava flow with a well-developed basal breccia. The second rhyolite unit, which has no other known exposures, is separated from the Shoshone Rhyolite by another ~ 170 m of basalt and sediment, and is referred to as the Kimberly Member of the Cassia Formation. It has been dated at 8.11 ± 0.05 and 7.95 ± 0.11 Ma (single grain sanidine $^{40}Ar/^{39}Ar$; Knott et al. 2016). This unit is approximately 180 m thick, and may be a densely welded ignimbrite (Knott et al. 2016), though we tentatively identify it as another lava flow because of its well-developed lower and upper breccias and lack of pyroclastic shards. Only a thin sediment horizon separates it from the lowermost unit, the Castleford Crossing Member (7.93 ± 0.48 Ma, single grain plagioclase $^{40}Ar/^{39}Ar$; Knott et al. 2016), which is interpreted as a welded ignimbrite. The Castleford Crossing Member has a minimum thickness of ~ 1400 m, and its base was not reached in the borehole (Fig. 2). Considering this thickness, we interpret this unit as a caldera-filling ignimbrite. Knott et al. (2016) estimate

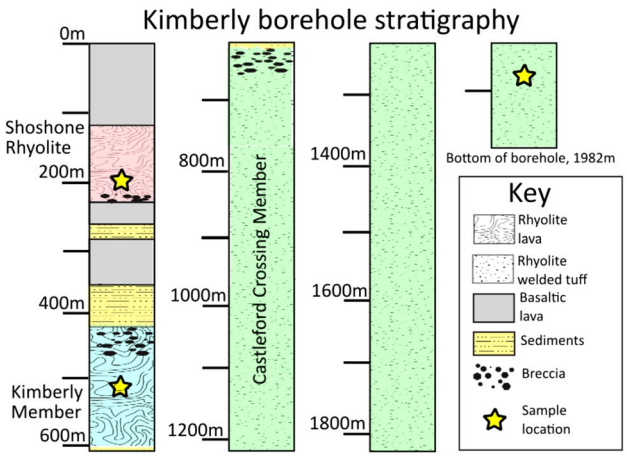

Fig. 2 Stratigraphy of the Kimberly Borehole, location shown in Fig. 1. The locations of sections of core used for this study are given by yellow stars, and are at depths of 218.2, 547.4, and 1888.8 m. For more detailed stratigraphy of the borehole and the surrounding region, see Knott et al. (2016)

based on regional exposures of the outflow facies of this unit that it represents an eruption of a minimum of 1900 km^3 of magma (dense rock equivalent), making it among the largest identified silicic eruptions produced by the Yellowstone hotspot. Finally, it should be noted that at least 10 additional ignimbrite outflow units underlie the Castleford Crossing Member in the Cassia Mountains just south of Twin Falls (Fig. 1); these range in age from 8.1 to 11.3 Ma, and likely originate from the Bruneau–Jarbidge and Twin Falls centers as well (Knott et al. 2016; Ellis et al. 2012), which means that the three rhyolitic deposits encountered by the Kimberly Borehole and sampled for our study probably represent only the later stages of the Twin Falls eruptive sequence.

Sample preparation and methods

Measurement of major phenocryst $\delta^{18}O$ values via laser fluorination

Major mineral phenocrysts (plagioclase, quartz, pyroxene) were extracted from crushed hand samples of welded ignimbrite using the methods described in Colón et al. (2015b). Zircon was isolated by either dissolution of the surrounding glass and phenocrysts in a 40% solution of hydrofluoric acid for the Bruneau–Jarbidge units or by separation in 3.2 g/cm^3 methylene iodide for the Twin Falls units. Oxygen isotopes in major phenocrysts were measured with an integrated laser fluorination-MAT-253 mass spectrometer system at the University of Oregon (Bindeman 2008), using BrF_5 as the fluorinating reagent. Samples were controlled for reproducibility via intercalibration with a UOG (+6.52‰ VSMOW) garnet standard measured relative to a Gore Mountain Garnet standard of +5.8‰ (Valley et al. 1995). Reproducibility of repeat measurements of standards was typically better than 0.2‰ (2 *s.d.*). When possible, measurements were made on multiple types of phenocrysts from each sample to rule out secondary alteration as a source of deviation from original magmatic $\delta^{18}O$ values.

Ion microprobe measurement of zircon $\delta^{18}O$ values

Zircon mount preparation was carried out at the Canadian Centre for Isotopic Microanalysis at the University of Alberta (CCIM, Twin Falls zircon, mount M1408) and at the Australian National University (Bruneau–Jarbidge zircon, mount M1402 = BF041), and secondary ion mass spectrometry (SIMS) measurements of zircon $\delta^{18}O$ were made at CCIM. Polished zircon mid-sections (though not necessarily the exact center of each grain) of unknowns and zircon reference materials were exposed within two 25-mm diameter epoxy mounts using diamond grits. The mounts were cleaned with a lab soap solution and de-ionized H_2O. The mounts were coated with 10 nm of high-purity Au prior to scanning electron microscopy (SEM) utilizing a Zeiss EVO MA15 instrument equipped with high-sensitivity, broadband cathodoluminescence and backscattered electron detectors. Beam conditions were 15 kV and 2–3 nA sample current. A further 40 nm of Au was subsequently deposited on the mount prior to SIMS analysis.

Oxygen isotopes (^{18}O, ^{16}O) in zircon were analyzed using a Cameca IMS 1280 multicollector ion microprobe. A $^{133}Cs^+$ primary beam was operated with impact energy of 20 keV and beam current of 2.0–2.5 nA. The ~10-µm diameter probe beam was rastered (20 × 20 µm) for 60–90 s prior to acquisition, and then 10 × 10 µm during acquisition, forming rectangular analyzed areas ~ 15 × 18 µm across and ~2 µm deep. The normal incidence electron gun was utilized for charge compensation. Negative secondary ions were extracted through 10 kV into the secondary (transfer) column. Transfer conditions included a 122-µm entrance slit, a 5 × 5-mm pre-ESA (field) aperture, and 100× sample magnification at the field aperture, transmitting all regions of the sputtered area. No energy filtering was employed. The mass/charge separated oxygen ions were detected simultaneously in Faraday cups L'2 ($^{16}O^-$) and H'2 ($^{18}O^-$) at mass resolutions (m/Δm at 10%) of 1950 and 2250, respectively. Secondary ion count rates for $^{16}O^-$ and $^{18}O^-$ were typically ~ 2.2×10^9 and 4.5×10^6 counts/s utilizing 10^{10} Ω and 10^{11} Ω amplifier circuits, respectively. Faraday cup baselines were measured at the start of the analytical session. A single analysis took 275 s, including pre-analysis rastering, automated secondary ion tuning, and 75 s of continuous peak counting.

Instrumental mass fractionation was monitored by repeated analysis of the zircon primary reference material (RM) after every four unknowns, either TEM2 ($\delta^{18}O_{VSMOW} = +8.2$‰; Black et al. 2004) for the Bruneau–Jarbidge samples, or S0081 (UAMT1; $\delta^{18}O = +4.87$; R. Stern, unpublished laser fluorination data, University of Oregon) for the Twin Falls zircon. TEM2 was also analyzed as a secondary RM on M1408 after every eight unknowns. The $^{18}O^-/^{16}O^-$ data set for the primary RM was processed collectively for each of three sessions ($N = 51$, 21, 40 for the Bruneau–Jarbidge and the two Twin Falls sessions, respectively), yielding standard deviations of 0.09‰–0.10‰, following correction for systematic within-session drift (≤0.4‰); overall instrumental mass fractionation was 1.1–1.8‰. The individual spot uncertainties for the unknowns at 95% confidence for $\delta^{18}O$ are derived from considering errors relating to within-spot counting statistics, between-spot (geometric) effects, and correction for instrumental mass fractionation, and average ±0.19‰, ±0.25‰, and ±0.20‰ for the three sessions, respectively. For the Bruneau–Jarbidge zircon, twelve analyzes of FC1 zircon (lacking a conventional reference value) yielded a weighted

mean $\delta^{18}O = +5.81 \pm 0.06$ (MSWD = 1.19). For the two sessions with the Twin Falls zircon, results for multiple spots on multiple grains of the secondary RM (TEM2) gave mean values for $\delta^{18}O = +8.21 \pm 0.11$ (MSWD = 1.3; $N = 9$, standard deviation = 0.14‰) and $+8.20 \pm 0.04$ (MSWD = 0.96; $N = 30$, standard deviation = 0.10‰), consistent with the reference value of +8.2‰ stated above (Black et al. 2004).

Laser ablation U–Pb dating and hf isotope analysis of zircons

Zircon grains were then analyzed at the University of California Santa Barbara via laser ablation multi-collector inductively coupled plasma mass spectrometry (LA-MC-ICP-MS) analysis (Kylander-Clark et al. 2013); these were selected to encompass the full diversity of zircon $\delta^{18}O$ values observed by SIMS. Grains were first dated via U–Pb spot analyses 15 µm wide and 5 µm deep (Fig. 3), using the TEM2 standard. 2σ uncertainties averaged 0.6 Ma for single spot analyses (see supplementary material). $^{206}Pb/^{238}U$ ages were corrected by measuring ^{207}Pb and using the correction for common Pb in ISOPLOT (Ludwig 2003).

Spots closely adjacent to the U–Pb age spots were then separately analyzed by LA-MC-ICP-MS in another session

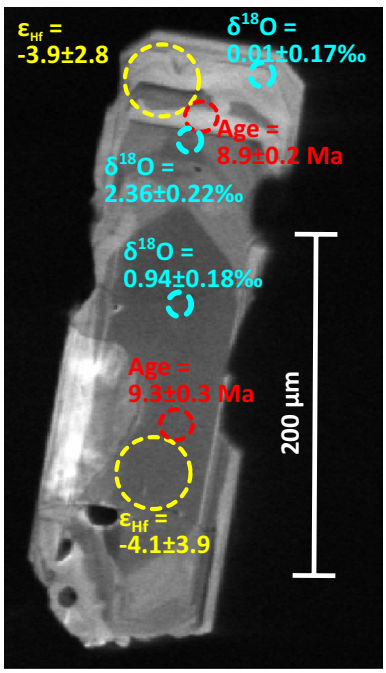

Fig. 3 Cathodoluminescence image of a complexly zoned zircon grain (#44, see supplementary material) from the Shoshone Rhyolite from the Kimberly borehole. Dashed circles show spot sizes of various analyses, including SIMS for $\delta^{18}O$ (~15 µm), U–Pb dates by LA-MC-ICP-MS (~15 µm, though they appear to have been slightly larger than SIMS spots on average), and 50 µm spot diameters for LA-MC-ICP-MS measurements of ε_{Hf} values. This grain was not dated by CA-ID-TIMS

(to achieve better precision than a split-stream analysis) for their Hf isotope composition, using 50 µm wide and 30 µm deep spots (Fig. 3) and using UAMT1 standards. 2σ uncertainties for each Hf isotope measurement averaged 3.6 ε units. Care was taken to keep laser ablation spots for both Hf and U–Pb spots as close as possible to the SIMS $\delta^{18}O$ spots so that analyses of the same zone of a single crystal could be compared (Figure III), which is especially important considering the intra-crystal variability in both isotopic compositions and ages (Figs. 4, 5). For this reason, we are able to pair zircon O and Hf isotope compositions of zircon cores and rims with the ages of those same regions of the crystal.

Thermal ionization mass spectrometry measurements of zircon

Finally, selected zircon crystals from the three Kimberly borehole units were extracted from epoxy grain mounts using stainless steel tools for high-precision dating via CA-ID-TIMS. Crystals were selected to encompass the entire range of laser ablation U–Pb ages and O and Hf isotopic compositions measured by the above methods, and care was taken (with one exception, see below) to avoid grains with noticeably different core and rim ages. As such, the distribution of ages derived from the TIMS data should be taken as representative of the ranges of ages of zircon grains in an individual eruption, but not as representative of the relative abundances of those ages (Fig. 5). Individual grains were annealed at 900 °C for 48 h, ultrasonically cleaned in 3N HNO_3 and loaded into Savillex microcapsules with a microdrop of 7N HNO_3 and 80 µl of concentrated HF for chemical abrasion (Mattinson 2005). Microcapsules were assembled in Parr bombs and zircon crystals were chemically abraded for 13 h at 180 °C. After chemical abrasion, zircon grains were transferred into 3 ml Savillex beakers, fluxed in 6N HCl and ultrasonically cleaned in 3N HNO_3. Cleaned single crystals were loaded back into their microcapsules with a microdrop of 7N HNO_3 and 60 µl of concentrated HF, spiked with 5 mg of EARHTIME ^{202}Pb-^{205}Pb-^{233}U-^{235}U tracer solution (Condon et al. 2015) and dissolved for 60 h at 210 °C in Parr bombs. After dissolution, samples were dried down and re-dissolved in 6N HCl at 180 °C overnight in Parr bombs. Samples were again dried down and re-dissolved in 3N HCl for anion exchange chemistry. Uranium and lead were separated from major and other trace elements using an HCl-based single-column anion-exchange chemistry modified from Krogh (1973) and U–Pb fractions were dried down with a drop of 0.02M H_3PO_4. Dried U–Pb fractions were loaded onto outgassed single Re-filaments with 1 µl of Si-Gel activator (Gerstenberger and Haase 1997). All analyses were performed at ETH Zürich employing a Thermo Scientific TRITON Plus thermal ionization mass spectrometer. Pb was analyzed using a dynamic peak-hopping routine on the axial

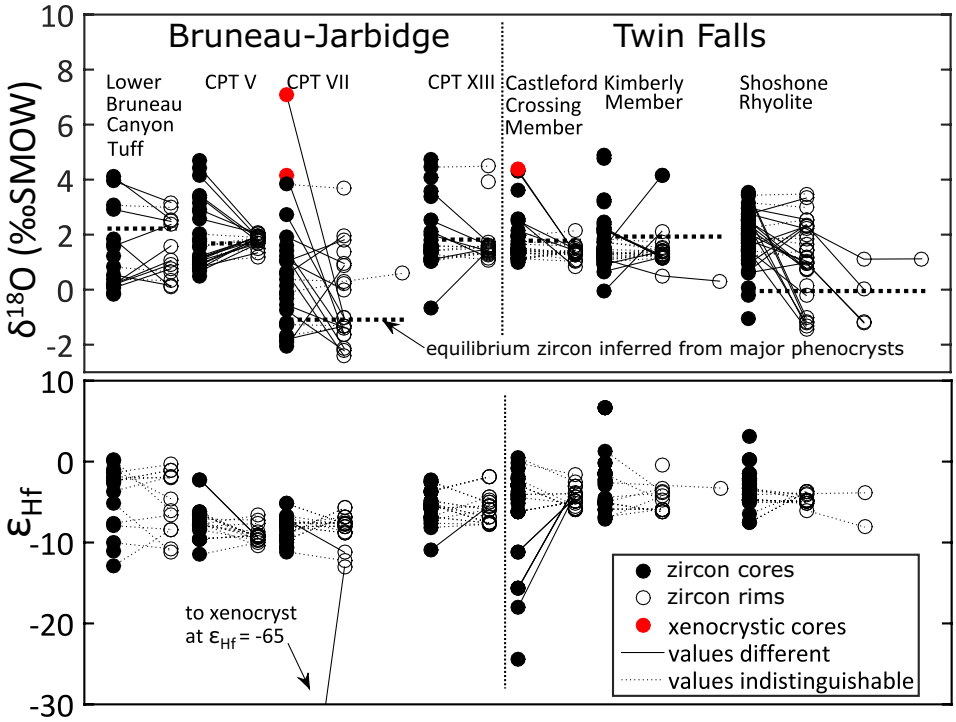

Fig. 4 Diversity in both hafnium and oxygen isotopes in zircon from all studied rhyolites. Core-rim pairs are connected by lines, solid where the two values do not overlap within their 2σ uncertainties, and are therefore resolvably different, and dashed otherwise. When more than one rim analysis was performed, the analyses farthest from the rim are plotted to the right. Zircon equilibrium compositions computed from major phenocrysts were inferred by subtracting 1.8‰ from quartz $\delta^{18}O$ values, 0‰ from pyroxene, or 1.0‰ from plagioclase (using fractionations from Loewen and Bindeman 2016), with the former minerals preferred when available. Note the much less diverse rims in CPT V which we interpret to be the result of batch mixing and overgrowth of rims in a well-mixed pre-eruptive magma chamber

secondary electron multiplier and U was measured as UO_2 using a static Faraday collection routine employing 10^{13} ohm resistors. Details concerning mass spectrometry and associated corrections are given in von Quadt et al. (2016) and Wotzlaw et al. (2017). U–Pb dates were calculated relative to the published calibration of the ET2535 tracer solution (Condon et al. 2015) and using the U-decay constants of Jaffey et al. (1971). $^{206}Pb/^{238}U$ dates were corrected for initial ^{230}Th-^{238}U disequilibrium using a constant Th–U partition coefficient ratio of 0.2 (see Wotzlaw et al. 2014 for details). We achieved average 2σ uncertainties of ~0.025 Ma with analytical uncertainties largely correlating with Pb^*/Pb_c (i.e., the ratio of radiogenic lead over common lead) and thus with uranium concentration. These uncertainties do not include systematic uncertainties associated with the tracer calibration and decay constants.

Results

Zircon ages

We obtained maximum estimates for eruption ages by taking the weighted mean of the largest population of statistically equivalent zircon rim LA-MC-ICP-MS ages from each sample (Fig. 5). All individual spot ages that differ by more than 95% confidence from the average age were excluded from the weighted averages, to remove the influence of antecrysts or zircon affected by Pb loss (Fig. 5, supplementary material). We only consider rim ages as many zircon cores are measurably older than the associated rim ages (Fig. 5, supplementary material), and thus cannot possibly reflect eruption ages. At Bruneau–Jarbidge, we propose an eruption age of 14.61 ± 0.15 Ma for the newly identified tuff of Bruneau Canyon, and ages of 11.96 ± 0.09 Ma for CPT V, 11.82 ± 0.10 Ma for CPT VII, and 10.68 ± 0.08 (all reported uncertainties are 2σ) for CPT XIII. The latter three are all indistinguishable from the $^{40}Ar/^{39}Ar$ ages previously reported by Bonnichsen et al. (2008, see above). At Twin Falls, we find zircon rim U–Pb ages of 7.96 ± 0.12 Ma for the Castleford Crossing Member, 7.70 ± 0.10 Ma for the Kimberly Member, and 6.06 ± 0.08 Ma for the Shoshone Rhyolite. All of these ages agree with the less precise $^{40}Ar/^{39}Ar$ ages given by Knott et al. (2016, see above), and we are able to distinguish the ages of the Kimberly and Castleford Members unlike in that study. This broad agreement with previous $^{40}Ar/^{39}Ar$ eruption ages suggests that our weighted average

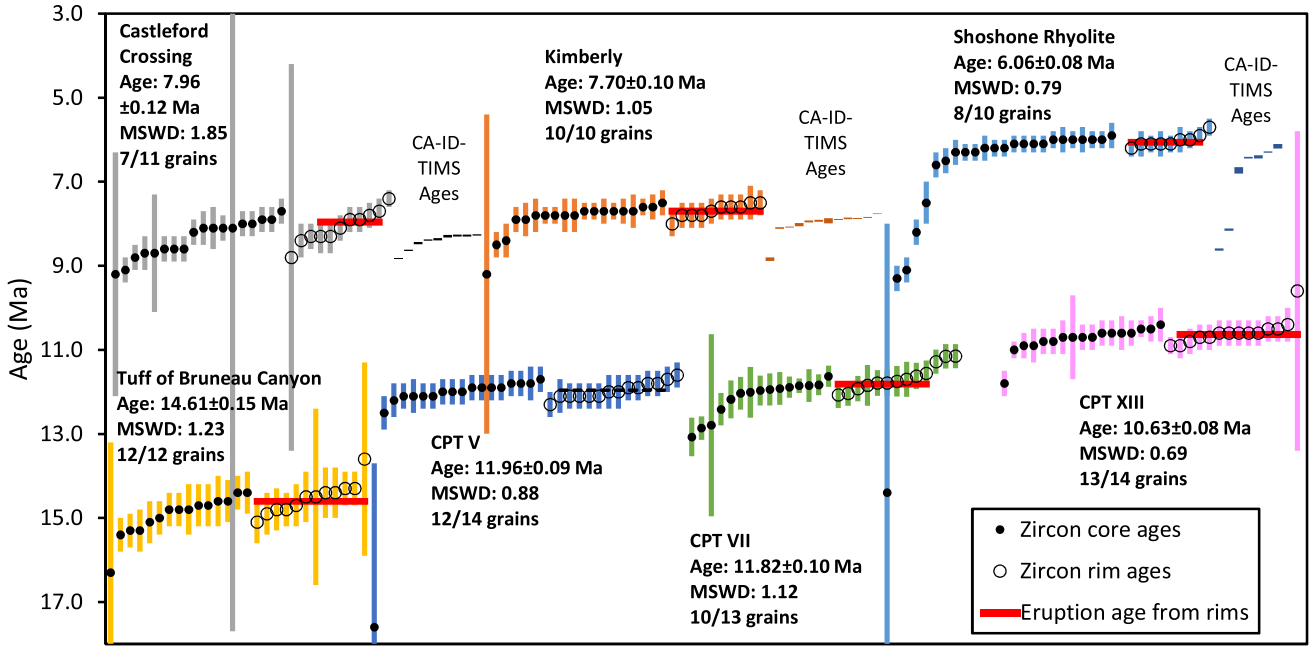

Fig. 5 Collection of all age data from this study. CA-ID-TIMS ages are all from the Twin Falls Kimberly borehole units (Fig. 2), and have much less uncertainty than the laser ablation ages (smaller vertical bars). Note that laser ablation-measured zircon rim ages are both younger and more homogeneous than the core ages. Horizontal red lines show the inferred eruption ages based on the rims, and cover the vertical error bars of the ages of the zircon used to compute those ages. All vertical age error bars are 2σ

zircon rim U–Pb ages accurately reflect the time of eruption of the magmas, giving us confidence that our age for the tuff of Bruneau Canyon, for which there is no $^{40}Ar/^{39}Ar$ age, also reflects the time of eruption of that unit.

With the 14.61 Ma tuff of Bruneau Canyon, we find clear evidence for volcanism significantly predating the 12.7 Ma $^{40}Ar/^{39}Ar$ age given by Bonnichsen et al. (2008) for the onset of volcanism at the Bruneau–Jarbidge center (with CPT III), again assuming that at least some zircon ages from each unit reflect eruption ages. This corroborates earlier results by Colón et al. (2015b), who dated three rhyolitic units exposed near Sheep Creek, some 20 km farther west of the Bruneau Canyon (the J-P Desert locality of Fig. 1), with ages ranging from 15.3 ± 0.4 Ma to 14.6 ± 0.4 Ma. The presence of a deposit of similar age in the Bruneau River Canyon to the east in the form of the tuff of Bruneau Canyon extends the mapped extent of units of this age, and corroborates that rhyolitic volcanism in the central Snake River Plain started shortly after the main phase of the Columbia River Basalts (Colón et al. 2015b; Coble and Mahood 2012), and continued for more than 9 Myr until the eruption of the Shoshone Rhyolite.

While the ages of our zircon rims are generally in good agreement with each other (Fig. 5), the populations of zircon core ages are not homogeneous in the cases of the three Kimberly borehole units, CPT VII, and the Tuff of Bruneau Canyon (Figs. 5, 6). Our high-precision TIMS dates of zircon from the Kimberly borehole (Figs. 5, 7, 8) define the age diversity of individual zircon grains within each unit more clearly than the lower-precision laser ablation dates (Fig. 5). We cross-checked the CA-ID-TIMS and LA-MC-ICP-MS dates for the zircon grains which were dated via both methods (Fig. 7). In nearly all cases, the CA-ID-TIMS and LA-MC-ICP-MS are equivalent within 2σ uncertainty. There are two zircon grains where this is not the case; one Castleford Crossing Member grain has a rim which is much younger than the core of the bulk grain (the only grain known to have significantly different core and rim ages which was dated by total dissolution), and one Kimberly Member grain has a CA-ID-TIMS age which is much older than either the core or rim age measured by LA-MC-ICP-MS. Despite these small inconsistencies, however, the general match achieved gives us confidence that the age distributions identified by the two methods are consistent. We also measured a few grains via CA-ID-TIMS for which we have $\delta^{18}O$ values but no laser ablation analyses (supplementary material). The single crystal ID-TIMS dates of isotopically diverse zircon resolve a prolonged history of magma production and recycling of older zircon. They span a range of 2.5 Myr for the Shoshone Rhyolite, 1.1 Myr for the Kimberly Member, and 0.6 Myr for the Castleford Crossing ignimbrite. These ranges far exceed the average 2σ analytical uncertainty which was ~0.025 Myr. They are also somewhat smaller than the age ranges obtained from LA-MC-ICP-MS analyses. This is

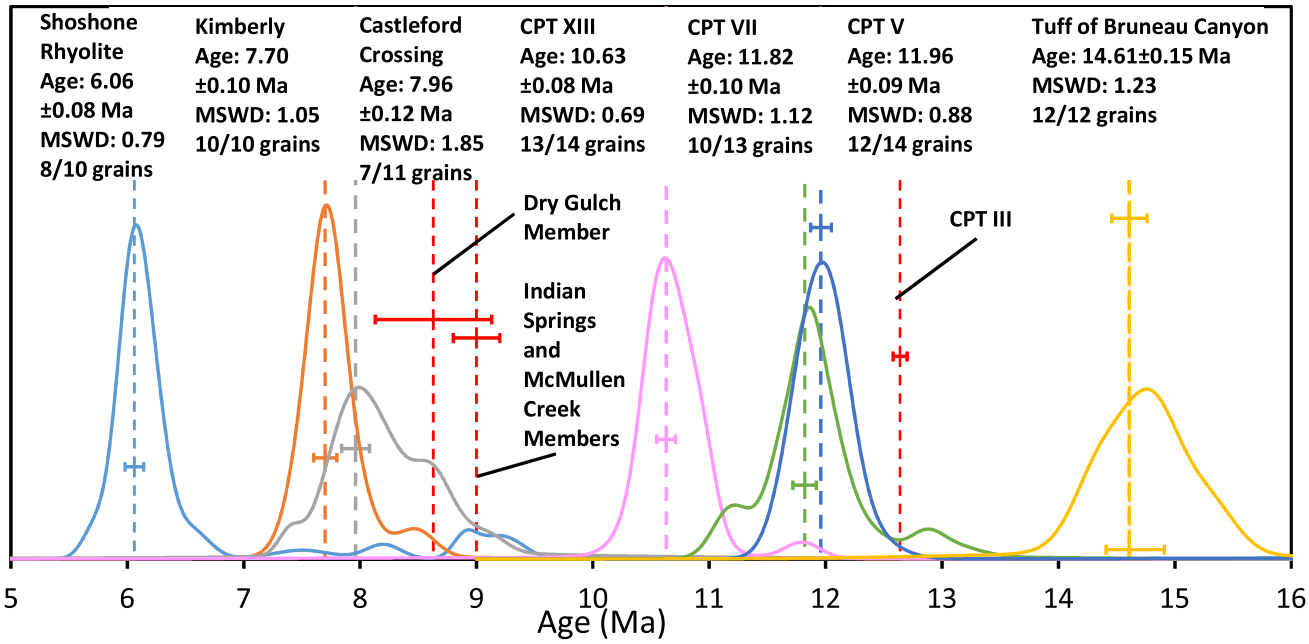

Fig. 6 Probability density curves for the zircon LA-MC-ICP-MS ages given in Fig. 5. The CA-ID-TIMS dates are not considered here, as they deliberately targeted non-representative zircon to characterize the full range of zircon ages, and would produce artificially wide peaks. Both core and rim ages contributed to these curves, but the eruption age estimates are calculated only from rims, as in Fig. 5. Curves were computed using ISOPLOT (Ludwig 2003). We also plot $^{40}Ar/^{39}Ar$ ages (as red dashed lines) from previous studies for four additional units, the Dry Gulch, Indian Springs, and McMullen Creek Members of the Cassia Formation at Twin Falls (Knott et al. 2016), and CPT III of Bruneau–Jarbidge (Bonnichsen et al. 2008)

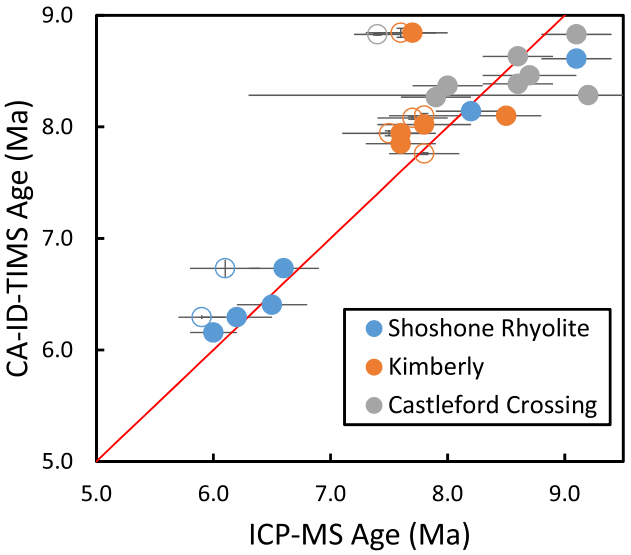

Fig. 7 Comparison of the two methods of dating zircon used in this study. Analyses made by laser ablation of rims are open circles, cores are closed. The red line is the 1:1 line; most of the ages fall on or near this line. All error bars are 2σ. This plot does not include five zircon grains that were dated via CA-ID-TIMS (all plotted in Fig. 8) that were not also analyzed by laser ablation

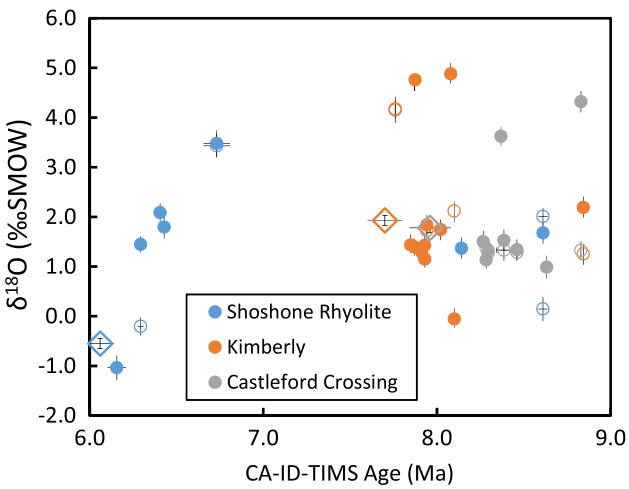

Fig. 8 Plot of all CA-ID-TIMS dates against the corresponding oxygen isotope measurements of the same zircon. Open circles represent cores and closed circles represent rims, which for a single zircon have matching whole-grain TIMS ages. Note the large range of ages, particularly in the Shoshone Rhyolite, and the large range of oxygen isotope compositions in magmas which were crystallizing zircon simultaneously in the crust, particularly in the rhyolite of the Kimberly Member at about 8 Ma, providing further evidence for the batch assembly process. Diamonds represent eruption ages (our estimates, Figs. 5, 6) paired with estimated equilibrium zircon values (horizontal lines in Fig. 4). All error bars are 2σ

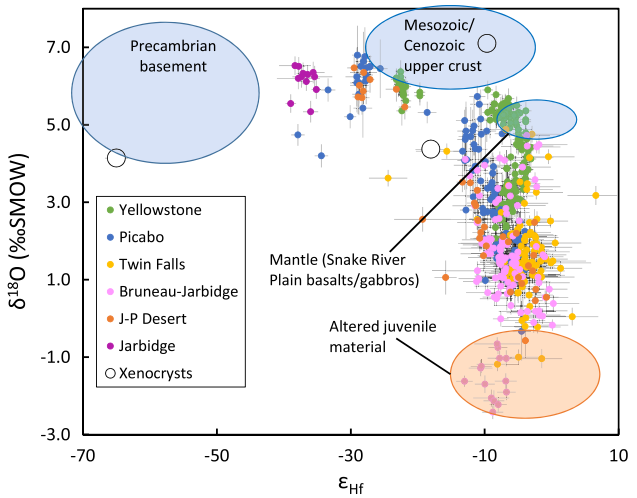

Fig. 9 Oxygen and hafnium isotopes in zircon from rhyolites throughout the Snake River Plain. Data sources for areas other than those covered in this study are Drew et al. (2013, Picabo), Colón et al. (2015b, Jarbidge and J-P Desert), Stelten et al. (2013), and Wotzlaw et al. (2015, both Yellowstone). The extent of the Mesozoic/Cenozoic Hf isotope range is inferred from Gaschnig et al. (2010), and the size of the Snake River Plain basalt field is from Stelten et al. (2017). We plot the J-P Desert zircon separately from the Bruneau–Jarbidge data from this study for the sake of clarity, though we interpret them as are part of the same system. Note the lack of zircon with low ε_{Hf} and $\delta_{18}O$ values, indicating a lack of mixing between those magma types, and suggesting that they did not form simultaneously, and that Precambrian rocks were not hydrothermally altered to a significant degree. We interpret the low-$\delta^{18}O$ end-member to be the result of syn-magmatic hydrothermal alteration of the young, unradiogenic, porous and hydrologically permeable gabbros and upper crust by a variety of mechanisms, in line with previous studies (e.g., Boroughs et al. 2012; Drew et al. 2013; Bindeman and Simakin 2014; Wotzlaw et al. 2015; Colón et al. 2015b). All error bars are 2σ

likely the result of the smaller number of zircon grains used for TIMS dates (Fig. 5), unintentional blending of core and rim ages, and the fact that we specifically avoided grains with different core and rim ages, and thus all of the zircon grains are identified to have old cores.

Oxygen and hafnium isotopes

Every one of the rhyolitic units analyzed in this study was depleted in $\delta^{18}O$ relative to normal melt values of ~ + 6.2 ± 0.3‰ (VSMOW) expected for a rhyolite derived from fractionation of mantle-derived basalts (e.g. Bindeman 2008). Calculated magmatic $\delta^{18}O$ values inferred from the compositions of major phenocrysts for the tuff of Bruneau Canyon, CPT V, CPT VII, and CPT XIII are + 3.5, + 3.8, + 0.2, and + 3.2‰, respectively (all uncertainties ± 0.2‰, these analyses were also reported in Bindeman and Simakin 2014, where the newly defined here tuff of Bruneau Canyon is labeled as CPT III, see sample 2005-ID-14). Amongst the Twin Falls units, we find magmatic $\delta^{18}O$ values based on major phenocrysts of + 2.3‰ for the Castleford Crossing Member, + 2.2‰ for the Kimberly Member, and − 0.6‰ for the Shoshone Rhyolite. Notably, the latter is one of the lowest $\delta^{18}O$ values obtained from major phenocrysts measured in any unit along the entire Snake River Plain–Yellowstone system. All seven units studied have significantly diverse oxygen isotope compositions in zircon. In all but the Shoshone Rhyolite, there is a greater range in $\delta^{18}O$ values in zircon cores than in zircon rims (Fig. 4), and the more homogeneous rim compositions tend to cluster around the bulk melt compositions inferred from the major phenocrysts, though in CPT VII and the tuff of Lower Bruneau Canyon this difference is admittedly small.

Similar complexity can be seen in the Hf isotope compositions of the zircon, though it is less resolvable than the diversity in the oxygen isotopes due to higher analytical error. We note several comparable trends, however, there are no samples with zircon rims that are more diverse than the corresponding cores, and we see significant reductions in diversity between cores and rims overall in the three studied Twin Falls units. This contrast is most pronounced in the Castleford Crossing Member, which has cores as low as ε_{Hf} -24 but no rims with ε_{Hf} less than − 6, and an upper limit of approximately $\varepsilon_{Hf} = 0$ in both cores and rims (Fig. 4).

Xenocrystic zircon

We identified only three xenocrystic (pre-Miocene) zircon cores in our entire dataset using laser ablation, all of which had young rims which closely matched the eruption ages of their respective host units (Fig. 4). In CPT VII, we found a single zircon core with an age of 86 ± 1.4 Ma, a $\delta^{18}O$ value of + 7.1 ± 0.18‰, and an ε_{Hf} value of − 9.7 ± 1.4, which we interpret based on its age and Hf isotopic composition as being derived from the Idaho Batholith (Gaschnig et al. 2010). The other two xenocrysts are Precambrian in age. One, which was also found in CPT VII, has an age of 1672 ± 24 Ma, a $\delta^{18}O$ value of + 4.14 ± 0.19‰, and an ε_{Hf} value of − 64 ± 1.7. The second Precambrian age comes from the Castleford Crossing Member, and has an age of 631 ± 21 Ma, a $\delta^{18}O$ value of + 4.37 ± 0.26‰, and an ε_{Hf} value of -18 ± 2.3. These cores all contrast significantly from their young rims in cathodoluminescence images, with the two Precambrian grains being exceptionally dark, with the Cretaceous core showing very fine oscillatory zoning which is absent in all the younger grains and is typical of intrusive zircon (e.g. Corfu et al. 2003).

Discussion

Recycling and inheritance of zircon grains

We find significant diversity in both LA-MC-ICP-MS and CA-ID-TIMS ages in the zircon from the three Kimberly borehole units, and, at Bruneau–Jarbidge, in the laser ablation ages from CPT VII and the tuff of Bruneau Canyon (Figs. 5, 6, 7, 8). Zircon grains which occur in the 6.06 Ma Shoshone Rhyolite range in age from the time of eruption to 9 Ma, a greater time span than the entire history of volcanism at the Yellowstone Plateau (Christiansen 2001). We additionally find that many zircon grains have rim LA-MC-ICP-MS spot ages that are measurably younger than the cores of those same crystals (Figs. 5, 7).

We identify three potential sources for this zircon age diversity. The first is that these zircon grains are merely incorporated into the volcanic deposit during the eruptive process, either from the sides of the conduits feeding the eruption or from the ground during the emplacement of pyroclastic flows. While we cannot rule this out for all zircon, we consider this explanation to be unlikely as the deposits we sampled lack significant visible xenoliths, and because several of the older zircon cores that we analyzed have rims that more closely mirror the eruption ages of the units that contain them (Fig. 5). This means that the zircon grains with older cores must have spent enough time in a younger magma to grow substantial rims, ruling out the possibility that they may have been derived from destroyed lithic fragments during an eruption.

The second possibility is that the older zircon grains were derived from previously erupted material which was deeply buried and partially remelted without destroying all the original zircon cores. The ≥ 1.5 km thickness of the 7.96-Ma castleford crossing member in the Kimberly borehole (Fig. 2), coupled with the existence of many older ignimbrite units that may be associated with the Twin Falls volcanic center (Knott et al. 2016), suggests that the cumulative depth of burial of the deepest intracaldera deposits of the earliest eruptions may be as much as 5 km. This puts these oldest ignimbrites and their constituent zircon well inside estimated depth range of the magma bodies which fuel the large ignimbrite eruptions throughout the Yellowstone hotspot track (e.g. Almeev et al. 2012; Bolte et al. 2015; Huang et al. 2015). This implies that the products of early caldera-forming eruptions at each volcanic center are recycled by processes of repeated caldera collapse, burial, melting, and re-eruption, perhaps even more than once in the case of the oldest eruptive deposits. The faulting associated with caldera collapse may also bring not just volcanic rocks, but also buried older intrusions into contact with hot intrusions that can melt them. This process has been implicated in the production of the low-$\delta^{18}O$ rhyolites which are ubiquitous throughout the Snake River Plain–Yellowstone system (Bindeman and Valley 2001; Bindeman and Simakin 2014; Colón et al. 2015b; Drew et al. 2013; Watts et al. 2011), as was discussed above.

The third possible source for the zircon age diversity is inheritance from older intrusions of the same volcanic center. Such grains would be antecrysts and are distinct from the much older and rarer xenocrysts discussed above. Given the long times between some of the zircon crystallization ages and their eruption ages, these source intrusions were probably mostly if not completely solidified prior to their remelting and incorporation into a younger magma chamber. This process is also the only possible source of antecrystic zircon found in the oldest ignimbrites at each locality, which formed before any deeply buried young volcanic rocks even existed (Fig. 10). All of these processes would tend to make the crystal cargo of each successive eruption more isotopically diverse, but it is also important to note that large scale melting and mixing of the magmatic system could destroy and effectively "reset" much of this variation, and we do not see any trend towards greater age diversity in later eruptions, with the sole possible exception of the Shoshone Rhyolite at Twin Falls (Figs. 5, 6).

Determining whether an individual zircon with a crystallization age that is resolvably older than an eruption age was inherited from an older intrusion or from buried volcanic rocks can be difficult. That said, we note a tantalizing correlation between the ages of antecrystic zircon grains at both Bruneau–Jarbidge and Twin Falls and the ages of prior eruptions. In Fig. 6, we plot four additional $^{40}Ar/^{39}Ar$ ages for eruptions not sampled in this study, the Dry Gulch, McMullan Creek, and Indian Springs Members of the Cassia Formation from Twin Falls, dated at 8.63 ± 0.50 Ma, 9.0 ± 0.3 Ma, and 9.0 ± 0.2 Ma, respectively (Knott et al. 2016), and CPT III from Bruneau–Jarbidge, dated via $^{40}Ar/^{39}Ar$ at 12.64 ± 0.08 by Bonnichsen et al. (2008). We see in Fig. 6 that the Shoshone Rhyolite has a notable antecrystic age peak that correlates with the 9.0 Ma age of the Indian Springs and McMullen Creek eruptions, and that the Castleford Crossing and Kimberly Members have zircon that also appear to match both the Dry Gulch and Indian Springs/McMullen Creek eruption ages. These peaks are represented by at least three core ages for each unit for each peak. Similarly, at Bruneau–Jarbidge we can see that CPT XIII has a secondary age peak (which is only one grain) which matches the ages of CPT XII and CPT V perfectly, and that CPT VII, in turn, has a secondary peak (corresponding to three grains) that matches the eruption age of CPT III.

Together, these observations build a compelling case that most zircon growth in the subvolcanic magma chambers occurs near the times of the eruptions, suggesting that

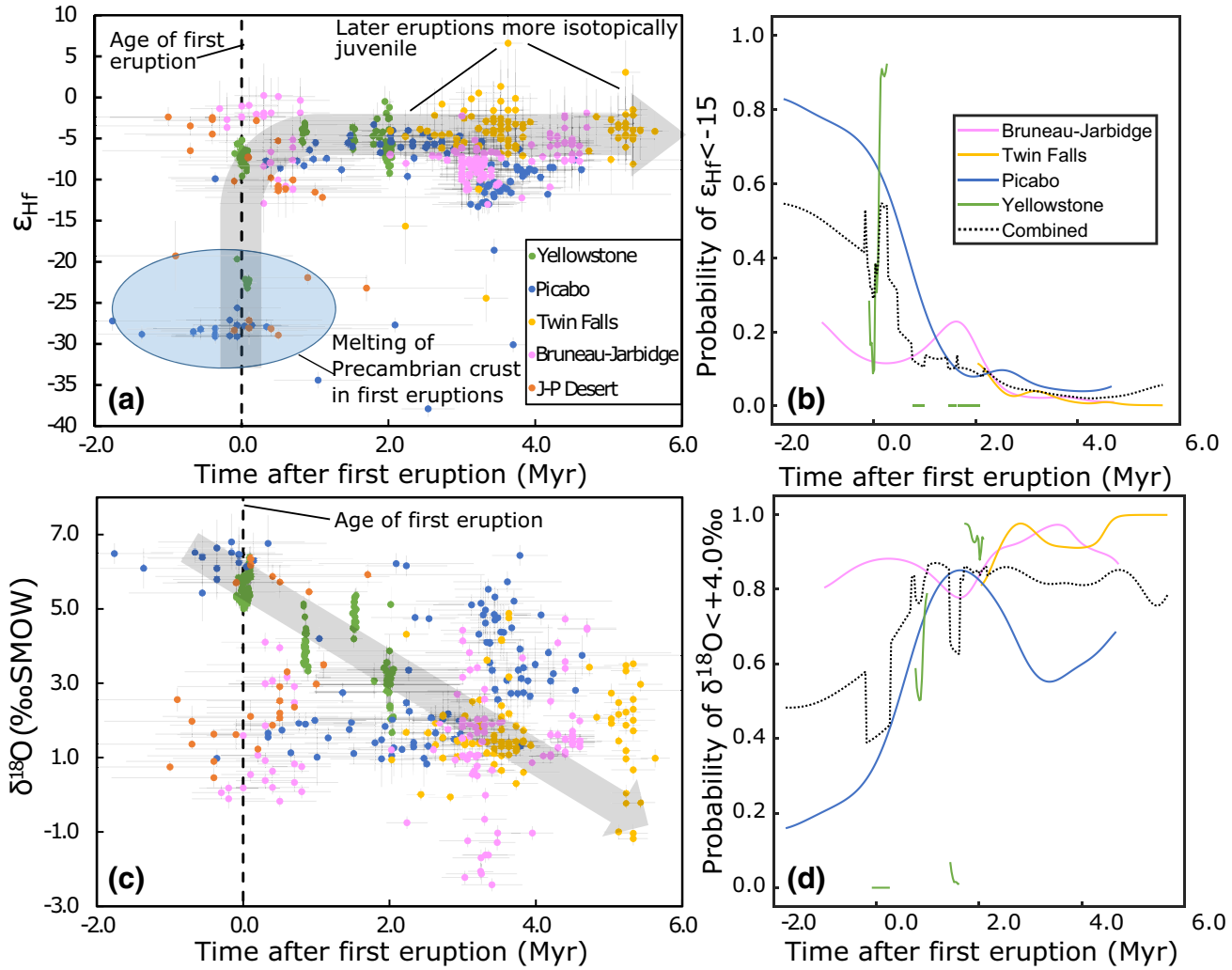

Fig. 10 **a** Hafnium isotopes vs. time after the oldest eruption at each major volcanic center along the Yellowstone-Snake River Plain hotspot track, using the same data sources as in Fig. 9. The Yellowstone, Bruneau–Jarbidge (which includes the J-P Desert), and Picabo centers all have their most unradiogenic (low-ε_{Hf}) zircon at the very beginning the cycle of activity, the only time in each magmatic cycle when the Precambrian crustal end-member is clearly discernable. We see few low-ε_{Hf} zircon crystals at Twin Falls; we speculate that this is because we did not study the earliest units from that center. We only include zircon analyses with age uncertainties less than 2 Myr (2σ). **b** Plot showing the probability that a zircon analysis at each studied eruptive center would give a low- ε_{Hf} (< -15) value as a function of its age, as in part (**a**). Note that in all cases this probability generally decreases with time. The Yellowstone curve is fragmented because the precise young age data (Wotzlaw et al. 2015) has gaps between eruptions. **c** Plot showing the oxygen isotopic compositions of zircon vs. time for the same set of zircon as in (**a**). **d** Plot showing the gradual increase in the likelihood of a zircon analysis being low-$\delta^{18}O$ ($<+4.0‰$) with time at each center. Here and in part (**c**) the combined curve is derived from averaging the other curves with equal weights. We note similar trends are documented in the one center not included here, the Heise center (Fig. 1; Drew et al. 2013; Nash et al. 2006; Szymanowski et al. 2016; Watts et al. 2011). All error bars in both panels are 2σ

magma production in the Snake River Plain is a punctuated rather than continuous process, and that eruptions are associated with these periods of increased magma production. To come to this conclusion, we assume that times of greater magma production are almost always recorded by populations of zircon ages, because the heating pulses associated with new intrusions and the growth of melt bodies should be associated with growth of zircon (either new crystals or adding to existing rims) during the subsequent cooling (Bindeman and Melnik 2016). Not all zircon ages match known eruption ages, however, and our very precise CA-ID-TIMS ages that we obtain for the Twin Falls units show that there are many zircon ages which are clearly older than their host eruptions but younger than the previous identified eruption (Figs. 5, 8), particularly in the case of the Shoshone Rhyolite. It is of course possible that these ages match those of small lava flows that are entirely concealed by younger deposits, but we argue that it is at least as likely

that at least some of them represent periods of intrusion which were not linked to any eruption. However, the fact that the overwhelming majority of zircon core and rim ages overlap with the ages of already identified eruptions suggests that most of these pulses of melt production were associated with eruptions. This assumes, of course, that intrusions of rhyolitic magma that never erupt are at least partially remolten and their zircon sampled by later intrusions that do produce eruptions. If there is a large body of rhyolitic intrusions at a totally different depth in the crust than the magma bodies that fuel eruptions, we would not expect to infer their compositions in this study. In summary, we expect that antecrystic zircon grains are almost certainly sometimes the result of the digestion of older intrusions which are frequently correlated with the ages of older eruptions, and perhaps sometimes inherited from the buried products of those older eruptions themselves.

The significant age diversity that we observe in several of these erupted units, including in the precise CA-ID-TIMS ages (Figs. 5, 7, 8), stands in contrast to the homogenous ages found in several previous high-precision CA-ID-TIMS studies of zircon from Yellowstone hotspot super-eruptions (Rivera et al. 2016; Szymanowski et al. 2016; Wotzlaw et al. 2014, 2015), where nearly all measured zircon ages from a given eruption are within 0.25 Myr of each other. We tentatively speculate that this is a result of two key differences between rhyolitic volcanism in the central Snake River Plain, and at Heise and Yellowstone. First, repose intervals between large ignimbrite eruptions in the central Snake River Plain (Bonnichsen et al. 2008; Knott et al. 2016; this study), at ~0.25 Myr, were much shorter than those at Heise and Yellowstone, where they have been 0.5–2.0 Myr (Christiansen 2001; Morgan and McIntosh 2005). Second, at any point in the 11−6 Ma time period, multiple caldera centers were simultaneously active (Bonnichsen et al. 2008), while in contrast activity at the Heise and Yellowstone systems since has been much more geographically focused. This suggests that the production of rhyolitic magma bodies in the central Snake River Plain was not only more frequent (e.g. Ellis et al. 2012, 2013) than in more recent times but was also more structurally complex and less centralized, possibly allowing populations of older zircon to survive more readily on the fringes of any new melt body.

Isotopic heterogeneity in zircon and batch assembly of pre-eruptive magma chambers

This greater geometric and temporal complexity in the central Snake River Plain is recorded not only by zircon ages but also by their O and Hf isotopic compositions. The range in zircon $\delta^{18}O$ values that we find in these rhyolitic units is among the greatest ever observed in any igneous rocks (Fig. 4) with ranges of up to 6.2‰ within a single unit (CPT VII), only rivaled by the Kilgore tuff of the Heise center (Wotzlaw et al. 2014). We see slightly less dramatic but still notable variability in the Hf isotopic composition of the grains, with most zircon grains having ε_{Hf} values scattered between 0 and − 10. Previous studies have found similar O and Hf isotope diversity at every major center of the Snake River Plain, and interpreted it as having formed through the assembly of "batches" of isotopically distinct melt bodies which existed for varying amounts of time prior to eruption (Bindeman and Simakin 2014; Colón et al. 2015a, b; Drew et al. 2013; Ellis and Wolff 2012; Szymanowski et al. 2016; Watts et al. 2011; Wotzlaw et al. 2014, 2015). We add the caveat that while the zircon crystals eventually reside within the same magma, some may be derived from solidified wall rocks rather than adjacent melt bodies to the parent magma, particularly in the case of zircon that are much older than the associated eruption ages. We see this in the plot of $\delta^{18}O$ vs. CA-ID-TIMS ages for the Shoshone Rhyolite zircon grains (Fig. 8), where the zircon closest to our inferred eruption age has a $\delta^{18}O$ value that overlaps with that estimated for the melt from major phenocrysts while older phenocrysts have very different $\delta^{18}O$ values. However, there are several cases where zircon have different isotopic compositions but have identical CA-ID-TIMS (or laser ablation) ages (Fig. 8), suggesting that at least some zircon diversity is derived from the mixing of coeval melt bodies, rather than the partial melting of separate previously solid intrusions.

We find additional evidence for the batch assembly of diverse melts in the core-rim relationships of zircon. In CPT V, we observe a large population of zircon rims and cores of indistinguishable age (Fig. 5), but the rims are significantly less diverse with respect to both Hf and O isotopes (Fig. 4), and we observe that the rim $\delta^{18}O$ values converge on the $\delta^{18}O$ value inferred for the melt from major phenocrysts, which are assumed to equilibrate with their host melts faster than zircon (Bindeman and Simakin 2014; Wotzlaw et al. 2014). Using the batch assembly model, we interpret these cores as recording the compositions of the early magma batches and the rims as recording the final eruptive melt composition, also reflected by major phenocryst oxygen isotopic composition. We also note that the time required to grow these zircon rims is likely much smaller than the age resolution of any of our dating methods, and was suggested to be on the order of 10^2–10^3 years by the modeling work of Bindeman and Melnik (2016). This convergence towards a common rim isotopic composition, seen most dramatically in CPT V and to a lesser extent in CPT XIII and in the Castleford Crossing Member, is in strong contrast with the equally diverse rims and cores observed in CPT VII and in the Shoshone Rhyolite, even amongst rims with indistinguishable ages. This suggests that either the zircon in these units mixed so rapidly in the final magma body that they did not have time to grow rims, or simply that there was not

a post-mixing cooling (or intrusion of Zr-rich magma) that oversaturated the magma in Zr and produced new zircon rims prior to eruption. In any case, we can constrain the speed of the batch assembly and eruption to be less than the typical 0.25 Myr uncertainty on our laser ablation ages, and we suspect that it may in fact occur much more quickly than that, in line with previous results for other centers along the hotspot track that have constrained it to occur in no more than 50 kyr (Wotzlaw et al. 2014, 2015). Such assembly of disparate melt bodies has been suggested by previous workers (Colón et al. 2015b; Wotzlaw et al. 2014, 2015) to possibly even be the trigger for the eventual volcanic eruption, as linking adjacent magma bodies may significantly alter the stress field of the surrounding crust, or allow volatiles to come out of solution and overpressurize the system. In the context of our study of the central Snake River Plain, this suggests that the pulses of rhyolitic magma production identified by zircon age peaks (Fig. 6) initially produce many isotopically distinct separate magma bodies, which then merge and erupt. In contrast, we find no evidence that magma bodies grow as a single isotopically homogeneous reservoir, and propose that the only way to produce large "supervolcanic" magma bodies in this kind of intraplate environment is through the progressive merging and mixing of smaller adjacent magma bodies.

Crustal sources of rhyolitic magmas

We compared the O and Hf isotope compositions that we observed in zircon from the Bruneau–Jarbidge and Twin Falls centers with data from four previous studies of other parts of the post-15 Ma hotspot track (Fig. 9, Colón et al. 2015b; Drew et al. 2013; Stelten et al. 2013; Wotzlaw et al. 2015). We find that the central Snake River Plain zircon analyses all fall along the compositional trend between the mantle end-member defined by the compositions of Snake River Plain and Yellowstone basalts, and the high-ε_{Hf} and low-$\delta^{18}O$ end-member discussed earlier, with CPT VII extending the lower bound in measurements of $\delta^{18}O$ from the hotspot track (Fig. 9, lowest gray points, supplementary material). While Colón et al. (2015b) found low-ε_{Hf} and normal-$\delta^{18}O$ zircon in precursor units to the Bruneau–Jarbidge center in the J-P Desert (orange points), we do not find any very low-ε_{Hf} zircon or, more importantly, any normal-$\delta^{18}O$ zircon in any of our Bruneau–Jarbidge or Twin Falls samples, confirming the exclusively low-$\delta^{18}O$ nature of the central Snake River Plain (Fig. 9).

This observation would seem to support the model of Boroughs et al. (2012), which asserts that the emplacement of the Idaho Batholith and later the Challis intrusions and volcanic rocks drove a regional-scale hydrothermal system which imparted low $\delta^{18}O$ values throughout the crust in the region of the central Snake River Plain, making any rhyolites generated by crustal melting in the central Snake River Plain also low-$\delta^{18}O$ in character. The involvement of Idaho Batholith-age protolith in the production of Bruneau–Jarbidge rhyolites is further suggested by the presence of an 86 Ma xenocryst in our CPT VII sample. This xenocryst has a normal $\delta^{18}O$ value, but we would not expect zircon to be affected by later hydrothermal alteration events. Its ε_{Hf} value, -9.7, is a match with the more radiogenic end of the Hf isotope composition of the low-$\delta^{18}O$ end-member, suggesting that it could be a source rock for many of the low-$\delta^{18}O$ rhyolites.

However, the fact that voluminous low-$\delta^{18}O$ rhyolites are found at every center along the hotspot track from eastern Oregon to Yellowstone strongly suggests that there is a process not dependent on any local geology that is responsible for a large portion of the low-$\delta^{18}O$ signature. High-ε_{Hf} and low-$\delta^{18}O$ zircon, particularly common at Bruneau–Jarbidge and Twin Falls (Fig. 9), are a better match in terms of Hf isotopes with Snake River Plain basalts, which have a minimum ε_{Hf} value of -8 (itself suggesting crustal contamination), than they are with the Idaho Batholith or the Challis, which have ε_{Hf} values which are generally less than -10 (Colón et al. 2015b; Gaschnig et al. 2010). This suggests that basaltic or rhyolitic intrusions or buried volcanic rocks of central Snake River Plain age were also being hydrothermally altered and melted along with older low-$\delta^{18}O$ material. This would tend to support the explanations for low-$\delta^{18}O$ rhyolites that depend on altered and buried intracaldera material (e.g. Bindeman and Valley; Watts et al. 2011; Drew et al. 2013) or on syn-volcanic alteration along local fault lines (Blum et al. 2016; Colón et al. 2015a, b; Drew et al. 2013).

Determining the relative amounts of hydrothermally altered and melted basalt/gabbro and Idaho Batholith/Challis-like upper crust is very difficult, as they are so isotopically similar with respect to their ε_{Hf} values both before and after alteration, and because variations in xenocryst compositions (Fig. 9) show that any simple mixing calculation using fixed end-members will likely be faulty. However, petrologic mass balances put upper limits on the volume of rhyolite that could have been derived from young basalts via fractionation and partial melting. If we assume that something on the order of 15 km of crustal thickening occurred in the Snake River Plain from basaltic intrusions (e.g. Peng and Humphreys 1998; McCurry and Rodgers 2008), and that it requires 90% fractionation (or 10% partial melting) of this material to produce rhyolite, then we arrive at a cumulative rhyolite thickness of 1.5 km in the Snake River Plain. The fact that the combined thickness of rhyolitic units in the Kimberly borehole meets or exceeds this value (Fig. 2), despite being an incomplete record of volcanism in the area, suggests that the cumulative thickness of erupted rhyolites is likely greater than 1.5 km, more than can be produced from basalts. This means that a significant portion of the low-$\delta^{18}O$

rhyolites in the central Snake River Plain can potentially be derived from partial melts of Mesozoic–Cenozoic upper crust that predates the Yellowstone hotspot. We again note, however, that caldera burial is not the only potential mechanism of hydrothermal alteration coeval with Yellowstone hotspot magmatism, and that the faulting and thermal conditions necessary to hydrothermally alter the crust existed in the central Snake River Plain since the time of the Columbia River Basalts (Blum et al. 2016; Colón et al. 2015b).

Time dependence of crustal reservoir contributions to erupted magmas

We observe that there is a distinct lack of zircon with simultaneously low-$\delta^{18}O$ and very low-ε_{Hf} compositions (Fig. 9). Wotzlaw et al. (2015) observed this pattern at Yellowstone, and interpreted it as the result of two-stage melting where the production of low-ε_{Hf} melts in the lower crust is followed by melting of shallow low-$\delta^{18}O$ crust in a separate system. We can now extend this observation to the entire hotspot track, which implies that it reflects a fundamental property of the melt generation processes along the hotspot track, and possibly in rhyolites that form in old continental crust in general. This lack of isotopically ancient low-$\delta^{18}O$ rocks is also observed at the Skaergaard intrusion in Greenland, where the fractured and permeable Tertiary gabbros are altered to low-$\delta^{18}O$ values but there is comparatively little oxygen isotopic alteration in the impermeable host Precambrian gneisses (Taylor and Forester 1979). Throughout the hotspot track, we argue that the lack of simultaneously low-$\delta^{18}O$ and low-ε_{Hf} rhyolites is likely a result of a combination of a two-step process, as proposed by Wotzlaw et al. (2015), and the impermeability-driven lack of alteration of Archean metamorphic rocks. Such rocks rarely outcrop on the surface in the region of the hotspot track (Drew et al. 2013) and, therefore, may not only be hard to alter but are also confined to depths below those typical of hydrothermal systems. Additionally, the low-$\delta^{18}O$ and low-ε_{Hf} magma end-members never appreciably mixed, as is recorded by the lack of hybrid-composition zircon, lending weight to the fact that the production of these magma types took place at different times.

In Fig. 10, we plot the ε_{Hf} and $\delta^{18}O$ values of all the zircon from the studies compiled in Fig. 9 against the difference between their age and the time of the earliest eruption at their respective source centers. When this difference is negative, it means that the zircon is older than the oldest identified eruption in the system, and reflects the growth of pre-volcanic magma chambers. We note that very low-ε_{Hf} grains only occur in significant numbers near and before the age of the oldest eruption, and quite rare after the first eruption at each volcanic center, especially if we exclude the off-axis Jarbidge rhyolite (distinct from Bruneau–Jarbidge, see Fig. 1), whose relationship to the main Snake River Plain sequence is debated (Brueseke et al. 2014; Colón et al. 2015b; Nash et al. 2006). We are not yet able to test for this trend in the Twin Falls zircon because the oldest zircon from that center has yet to be measured for Hf isotopes. While the precise composition of the Precambrian crustal end-member is unconstrained, we can use changes in the hafnium isotopic composition of each center's zircon population with time as a crude proxy for the amount of old crust which was melting to produce the erupted rhyolites at that time. This leads us to conclude that the melting of Precambrian crust is important for the initial stages of volcanism at each area (e.g. the Arbon Valley Tuff at Picabo; Drew et al. 2013, 2016) and diminishes over time as the zircon in later rhyolites become less like the Precambrian crustal end-member. At the one center not included in Fig. 10, Heise, a similar gradual increase in ε_{Nd} values with time has been documented by Nash et al. (2006). Late-stage rhyolites must still have a very large component of crustal melting, as they do not resemble the mantle end-member in their $\delta^{18}O$ values. Therefore, the crust which melts to produce the late-stage rhyolites of the Snake River Plain/Yellowstone volcanic systems is likely some combination of hydrothermally altered shallow crust and volcanic rocks and juvenile basaltic and rhyolitic intrusions, whereas the Precambrian crustal end-member becomes increasingly diluted as the system evolves (Fig. 10).

We also note that there is a common trend of evolution towards lower $\delta^{18}O$ values in the zircon from each center over time, most dramatically in those from Yellowstone (Stelten et al. 2013; Wotzlaw et al. 2015). This trend is visible to a lesser degree in the Bruneau–Jarbidge zircon if we include the J-P Desert units in the Bruneau–Jarbidge center, as is suggested by Colón et al. (2015b). This suggests that at least some of the processes that produced low-$\delta^{18}O$ crust that melted to become new rhyolites continued while the system was active, providing additional evidence that some combination of caldera burial-driven recycling and alteration along normal faults continued coeval with volcanism in the central Snake River Plain and that low-$\delta^{18}O$ values there are not solely the result of pre-existing alteration (Boroughs et al. 2012).

In Fig. 11, we illustrate how early intrusions of basalt from the mantle at each center could melt significant quantities of older crust. By contrast, later intrusions encounter an environment filled with these early basaltic intrusions or with rhyolitic material that has been buried by successive volcanic collapses. Once each caldera center becomes more mature, as seen in the lower part of the figure, the density of the early basaltic intrusions allows new basalt intrusions to buoyantly rise into the growing sill complex, or to even reach its top where it meets the rhyolitic magma chamber. If, as we suspect, ancient Precambrian rocks are primarily concentrated in the mid to lower crust (as suggested by Colón

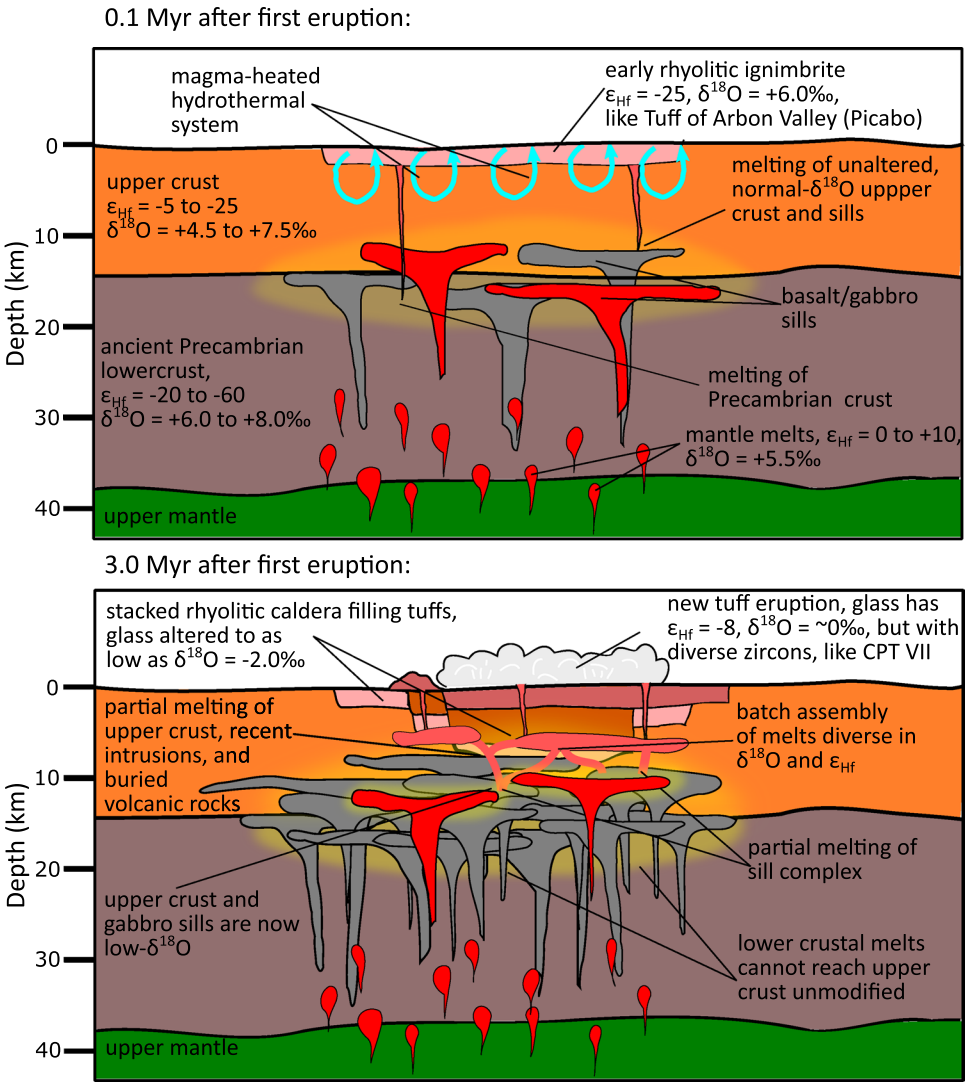

Fig. 11 Conceptual model of Snake River Plain caldera volcanism to explain the isotopic evolution seen in Figs. 9 and 10. Early Snake River Plain-Yellowstone rhyolites at each center are produced with large amounts of assimilation of old pre-existing crust, giving the products of the first eruptions normal $\delta^{18}O$ values and low ε_{Hf} values. By the late stage, new partial melting is mostly confined to the upper crust, and old solidified sills isolate the Precambrian crust from the melt bodies, which have been displaced to slightly shallower levels. Late stage ignimbrites and rhyolite lavas are isotopically juvenile and low-$\delta^{18}O$

et al. 2015b; Drew et al. 2013, 2016; Foster et al. 2006), this means that later basalt intrusions will likely be isolated from it and will not melt it efficiently (Fig. 11). Furthermore, any melts of ancient Precambrian crust that do form in the late stages of the system may be too hot to be crystallizing zircon, and may also not be able to rise through the mid-crustal sill system without hybridizing with more radiogenic melts to the point where their Archean-like Hf isotope composition is lost.

Conclusions

(1) We find considerable ranges in the ages and isotopic compositions of zircon from the Bruneau–Jarbidge and Twin Falls volcanic centers of the central Snake River Plain, implying that their source magmas were a diverse combination of partial melts of coeval basalt intrusions and their differentiates, of buried volcanic rocks from the same system, and of pre-existing crust. (2) This pre-existing crust can be roughly separated into two isotopically distinct end-members which are the ancient Precambrian basement rock, and the intrusions and volcanic rocks of the Idaho Batholith and Challis formations. (3) Combinations of the latter and young basaltic intrusions were progressively altered to lower $\delta^{18}O$ values by hydrothermal systems driven by heat from hotspot magmatism. Mixing between these crustal end-members was characterized by an early stage of magmatism where isotopically mantle-like melts hybridized with both ancient Precambrian crust and isotopically younger but mostly normal-$\delta^{18}O$ upper crust and a later stage where melting is dominated by shallow hydrothermally altered low-$\delta^{18}O$ material and the Precambrian end-member becomes nearly undetectable. (4) We also find no evidence that the Precambrian crust itself became significantly hydrothermally altered, presumably because it occurs at greater depths and/or has a much lower permeability that prevents it from being accessed by hydrothermal fluids. (5) Populations of zircon ages from these

units are diverse, and suggest that magma production in the central Snake River Plain was an intermittent process characterized by pulses of rhyolite production which appears to have usually led to eruption, preserving zircon O and Hf isotopic diversity. These pulses of magma production were characterized first by the formation of many closely spaced but isotopically distinct batches of melt which later merged into a single magma body prior to eruption. In some cases, particularly CPT V at Bruneau–Jarbidge, this final magma body's composition is recorded by the rims of the zircon, which like the rim ages, are much more homogeneous than the associated zircon cores. (6) We suggest that these two processes of (i) rapid batch assembly of separate bodies of melt prior to supervolcanic eruptions and increasingly shallow melting and (ii), vigorous syn-magmatic hydrothermal alteration leading to the coeval production of low-$\delta^{18}O$ rhyolites characterizes similar low-$\delta^{18}O$ anorogenic, intraplate, rift, and hot-spot rhyolitic provinces worldwide, because we can now confirm that these processes occur throughout the Yellowstone hotspot track, suggesting that they not solely function of the variable local geology.

Acknowledgements We thank Bin Fu for making one of the zircon mounts, Andrew Kylander-Clark at the University of California-Santa Barbara for the LA-MC-ICP-MS analyses for this study, and Jim Palandri for his measurements of major phenocryst $\delta^{18}O$ values at the University of Oregon. The Kimberly borehole was part of Project Hotspot, led by J. Shervais and funded by the US Department of Energy and the International Continental Drilling Program. Funding for this project was provided by the NSF grant EAR1447337, the University of Oregon Earth Science Department Staples Fellowship, and the ETH Zürich Postdoctoral Fellowship Program. We would finally like to thank three anonymous reviewers for their constructive criticisms of this manuscript.

References

Almeev RR, Bolte T, Nash BP, Holtz F, Erdmann M, Cathey HE (2012) High-temperature, low-H_2O silicic magmas of the yellowstone hotspot: an experimental study of rhyolite from the Bruneau-Jarbidge eruptive center, Central Snake River Plain, USA. J Petrol 53:1837–1866. https://doi.org/10.1093/petrology/egs035

Anders MH, Rodgers DW, Hemming SR, Saltzman J, DiVenere VJ, Hagstrum JT, Embree GF, Walter RC (2014) A fixed sublithospheric source for the late Neogene track of the Yellowstone hotspot: implications of the Heise and Picabo volcanic fields. J Geophys Res Solid Earth 119:2871–2906. https://doi.org/10.1002/2013JB010483

Archibald DB, Collins AS, Foden JD, Payne JL, Holden P, Razakamanana T, De Waele B, Thomas RJ, Pitfield PEJ (2016) Genesis of the Tonian Imorona-Itsindro magmatic Suite in central Madagascar: insights from U-Pb, oxygen and hafnium isotopes in zircon. Precambrian Res 281:312–337. https://doi.org/10.1016/j.precamres.2016.05.014

Bindeman I (2008) Oxygen isotopes in mantle and crustal magmas as revealed by single crystal analysis. Rev Miner Geochem 69:445–478. https://doi.org/10.2138/rmg.2008.69.12

Bindeman IN, Melnik OE (2016) Zircon survival, rebirth and recycling during crustal melting, magma crystallization, and mixing based on numerical modelling. J Petrol 57:437–460. https://doi.org/10.1093/petrology/egw013

Bindeman IN, Simakin AG (2014) Rhyolites-hard to produce, but easy to recycle and sequester: integrating microgeochemical observations and numerical models. Geosphere 10:930–957. https://doi.org/10.1130/GES00969.1

Bindeman IN, Valley JW (2001) Low-delta O-18 rhyolites from Yellowstone: magmatic evolution based on analyses of zircons and individual phenocrysts. J Petrol 42:1491–1517. https://doi.org/10.1093/petrology/42.8.1491

Bindeman I, Gurenko A, Carley T, Miller C, Martin E, Sigmarsson O (2012) Silicic magma petrogenesis in Iceland by remelting of hydrothermally altered crust based on oxygen isotope diversity and disequilibria between zircon and magma with implications for MORB. Terra Nov 24:227–232. https://doi.org/10.1111/j.1365-3121.2012.01058.x

Black LP, Kamo SL, Allen CM, Davis DW, Aleinikoff JN, Valley JW, Mundil R, Campbell IH, Korsch RJ, Williams IS, Foudoulis C (2004) Improved 206Pb/238U microprobe geochronology by the monitoring of a trace-element-related matrix effect; SHRIMP, ID-TIMS, ELA-ICP-MS and oxygen isotope documentation for a series of zircon standards. Chem Geol 205:115–140. https://doi.org/10.1016/j.chemgeo.2004.01.003

Blum TB, Kitajima K, Nakashima D, Valley JW (2016) Oxygen isotope evolution of the Lake Owyhee volcanic field, Oregon, and implications for the low-$\delta^{18}O$ magmatism of the Snake River Plain-Yellowstone hotspot and other low-$\delta^{18}O$ large igneous provinces. Contrib Miner Petrol 171:92. https://doi.org/10.1007/s00410-016-1297-x

Bolte T, Holtz F, Almeev R, Nash B (2015) The Blacktail Creek Tuff: an analytical and experimental study of rhyolites from the Heise volcanic field, Yellowstone hotspot system. Contrib Miner Petrol 169:15. https://doi.org/10.1007/s00410-015-1112-0

Bonnichsen B, Citron GP (1982) The Cougar Point Tuff, Southwestern Idaho and Vicinity. Cenozoic Geol Idaho Bureau Mines Geol Bull 26:255–281

Bonnichsen B, Leeman WP, Honjo N, McIntosh WC, Godchaux MM (2008) Miocene silicic volcanism in southwestern Idaho: geochronology, geochemistry, and evolution of the central Snake River Plain. Bull Volcanol 70:315–342. https://doi.org/10.1007/s00445-007-0141-6

Boroughs S, Wolff JA, Ellis BS, Bonnichsen B, Larson PB (2012) Evaluation of models for the origin of Miocene low-$\delta^{18}O$ rhyolites of the Yellowstone/Columbia River Large Igneous Province. Earth Planet Sci Lett 313–314:45–55. https://doi.org/10.1016/j.epsl.2011.10.039

Brueseke ME, Callicoat JS, Hames W, Larson PB (2014) Mid-Miocene rhyolite volcanism in northeastern Nevada: the Jarbidge rhyolite and its relationship to the Cenozoic evolution of the northern Great Basin (USA). Bull Geol Soc Am 126:1047–1067. https://doi.org/10.1130/B30736.1

Cathey HE, Nash BP (2004) The Cougar Point Tuff: implications for Thermochemical zonation and longevity of high-temperature, large-volume silicic magmas of the miocene Yellowstone hotspot. J Petrol 45:27–58. https://doi.org/10.1093/petrology/egg081

Cathey HE, Nash BP, Seligman AN, Valley JW, Kita N, Allen CM, Campbell IH, Vazquez JA, Wooden JL (2011) Low $\delta^{18}O$ zircons from the Bruneau-Jarbidge eruptive center: a key to crustal anatexis along the track of the Yellowstone hotspot. In 2011 Fall Meeting, American Geophysical Union, 5–9 December 2011, San Francisco, CA

Christiansen RL (2001) The Quaternary and Pliocene Yellowstone Plateau volcanic field of Wyoming, Idaho, and Montana. U S Geol Surv Prof Pap 729–G:145

Christiansen EH, McCurry M (2008) Contrasting origins of Cenozoic silicic volcanic rocks from the western Cordillera of the United States. Bull Volcanol 70:251–267. https://doi.org/10.1007/s00445-007-0138-1

Coble MA, Mahood GA (2012) Initial impingement of the Yellowstone plume located by widespread silicic volcanism contemporaneous with Columbia River flood basalts. Geology 40:655–658. https://doi.org/10.1130/G32692.1

Colón DP, Bindeman IN, Stern RA, Fisher CM (2015a) Isotopically diverse rhyolites coeval with the Columbia River Flood Basalts: evidence for mantle plume interaction with the continental crust. Terra Nov 27:270–276. https://doi.org/10.1111/ter.12156

Colón DP, Bindeman IN, Ellis BS et al (2015b) Hydrothermal alteration and melting of the crust during the Columbia River Basalt-Snake River Plain transition and the origin of low-$\delta^{18}O$ rhyolites of the central Snake River Plain. Lithos 224–225:310–323. https://doi.org/10.1016/j.lithos.2015.02.022

Condon DJ, Schoene B, McLean NM, Bowring SA, Parrish RR (2015) Metrology and traceability of U-Pb isotope dilution geochronology (EARTHTIME Tracer Calibration Part I). Geochim Cosmochim Acta 164:464–480. https://doi.org/10.1016/j.gca.2015.05.026

Corfu F, Hanchar JM, Hoskin PWO, Kinny P (2003) Atlas of Zircon Textures. Rev Mineral Geochemistry 53:469–500. https://doi.org/10.2113/0530469

Couper S (2016) Dual multicollector laser ablation split stream mass spectrometry: Application to the Bruneau-Jarbidge volcanic center, central Snake River Plain, Idaho. M.S. Thesis, University of Utah

Curtis CG, Harris C, Trumbull RB, De Beer C, Mudzanani L (2013) Oxygen isotope diversity in the anorogenic Koegel Fontein complex of South Africa: a case for basement control and selective melting for the production of low-$\delta^{18}O$ magmas. J Petrol 54:1259–1283. https://doi.org/10.1093/petrology/egt011

Drew DL, Bindeman IN, Watts KE, Schmitt AK, Fu B, McCurry M (2013) Crustal-scale recycling in caldera complexes and rift zones along the Yellowstone hotspot track: O and Hf isotopic evidence in diverse zircons from voluminous rhyolites of the Picabo volcanic field, Idaho. Earth Planet Sci Lett 381:63–77. https://doi.org/10.1016/j.epsl.2013.08.007

Drew DL, Bindeman IN, Loewen MW, Wallace PJ (2016) Initiation of large-volume silicic centers in the Yellowstone hotspot track: insights from H_2O- and F-rich quartz-hosted rhyolitic melt inclusions in the Arbon Valley Tuff of the Snake River Plain. Contrib Miner Petrol 171:1–20. https://doi.org/10.1007/s00410-015-1210-z

Ellis BS, Wolff JA (2012) Complex storage of rhyolite in the central Snake River Plain. J Volcanol Geotherm Res 211–212:1–11. https://doi.org/10.1016/j.jvolgeores.2011.10.002

Ellis BS, Branney MJ, Barry TL, Barfod D, Wolff JA, Bonnichsen B (2012) Geochemical correlation of three large-volume ignimbrites from the Yellowstone hotspot track, Idaho, USA. Bull Volcanol 74:261–277. https://doi.org/10.1007/s00445-011-0510-z

Ellis BS, Wolff JA, Boroughs S, Mark DF, Starkel WA, Bonnichsen B (2013) Rhyolitic volcanism of the central Snake River Plain: a review. Bull Volcanol 75:1–19. https://doi.org/10.1007/s00445-013-0745-y

Ferns ML, McClaughry JD (2013) Stratigraphy and volcanic evolution of the middle Miocene to Pliocene La Grande-Owyhee eruptive axis in eastern Oregon. Geol Soc Am Spec Pap 497:401–427. https://doi.org/10.1130/2013.2497(16).

Foster DA, Mueller PA, Mogk DW, Wooden JL, Vogl JJ (2006) Proterozoic evolution of the western margin of the Wyoming craton: implications for the tectonic and magmatic evolution of the northern Rocky Mountains. Can J Earth Sci 43:1601–1619. https://doi.org/10.1139/e06-052

Fu B, Kita NT, Wilde SA, Liu X, Cliff J, Greig A (2013) Origin of the Tongbai-Dabie-Sulu Neoproterozoic low-$\delta^{18}O$ igneous province, east-central China. Contrib Miner Petrol 165:641–662. https://doi.org/10.1007/s00410-012-0828-3

Gaschnig RM, Vervoort JD, Lewis RS, McClelland WC (2010) Migrating magmatism in the northern US Cordillera: In situ U-Pb geochronology of the Idaho batholith. Contrib Miner Petrol 159:863–883. https://doi.org/10.1007/s00410-009-0459-5

Gautason B, Muehlenbachs K (1998) Oxygen isotopic fluxes associated with high-temperature processes in the rift zones of Iceland. Chem Geol 145:275–286. https://doi.org/10.1016/S0009-2541(97)00148-4

Gerstenberger H, Haase G (1997) A highly effective emitter substance for mass spectrometric Pb isotope ratio determinations. Chem Geol 136:309–312. https://doi.org/10.1016/S0009-2541(96)00033-2

Harris C, Ashwal LD (2002) The origin of low $\delta^{18}O$ granites and related rocks from the Seychelles. Contrib Miner Pet 143:366–376. https://doi.org/10.1007/s00410-002-0349-6

Harris C, Erlank AJ (1992) The production of large-volume, low-$\delta^{18}O$ rhyolites during the rifting of Africa and Antarctica: the Lebombo Monocline, southern Africa. Geochim Cosmochim Acta 56:3561–3570. https://doi.org/10.1016/0016-7037(92)90399-4

Hiess J, Bennett VC, Nutman AP, Williams IS (2011) Archaean fluid-assisted crustal cannibalism recorded by low $\delta^{18}O$ and negative εHf(T)isotopic signatures of West Greenland granite zircon. Contrib Miner Pet 161:1027–1050. https://doi.org/10.1007/s00410-010-0578-z

Hildreth W, Christiansen RL, O'Neil JR (1984) Catastrophic isotopic modification of rhyolitic magma at times of caldera subsidence, Yellowstone Plateau Volcanic Field. J Geophys Res 89:8339–8369. https://doi.org/10.1029/JB089iB10p08339

Hildreth W, Halliday AN, Christiansen RL (1991) Isotopic and chemical evidence concerning the genesis and contamination of basaltic and rhyolitic magma beneath the Yellowstone plateau volcanic field. J Petrol 32:63–138. https://doi.org/10.1093/petrology/32.1.63

Huang H-H, Lin F-C, Schmandt B, Farrell J, Smith RB, Tsai VC (2015) The Yellowstone magmatic system from the mantle plume to the upper crust. Science 348:773–776. https://doi.org/10.1126/science.aaa5648

Jaffey AH, Flynn KF, Glendenin LE, Bentley WCT, Essling AM (1971) Precision measurement of half-lives and specific activities of U235 and U238. Phys Rev C 4:1889–1906. https://doi.org/10.1103/PhysRevC.4.1889

Knott TR, Branney MJ, Reichow MK, Finn DR, Coe RS, Storey M, Barfod D, McCurry M (2016) Mid-Miocene record of large-scale Snake River-type explosive volcanism and associated subsidence on the Yellowstone hotspot track: the Cassia Formation of Idaho, USA. Bull Geol Soc Am 128:1121–1146. https://doi.org/10.1130/B31324.1

Krogh TE (1973) A low-contamination method for hydrothermal decomposition of zircon and extraction of U and Pb for isotopic age determinations. Geochim Cosmochim Acta 37:485–494. https://doi.org/10.1016/0016-7037(73)90213-5

Kylander-Clark ARC, Hacker BR, Cottle JM (2013) Laser-ablation split-stream ICP petrochronology. Chem Geol 345:99–112. https://doi.org/10.1016/j.chemgeo.2013.02.019

Leeman WP, Menzies MA, Matty DJ, Embree GF (1985) Strontium, neodymium and lead isotopic compositions of deep crustal xenoliths from the Snake River Plain: evidence for Archean basement. Earth Planet Sci Lett 75:354–368. https://doi.org/10.1016/0012-821X(85)90179-7

Leeman WP, Oldow JS, Hart WK (1992) Lithosphere-scale thrusting in the western US Cordillera as constrained by Sr and Nd isotopic transitions in Neogene volcanic rocks. Geology 20:63–66

Loewen M, Bindeman IN (2016) Oxygen isotope thermometry reveals high magmatic temperatures and petrogenetic differences between hot-dry Yellowstone/ Snake River Plain and Icelandic rhyolites compared to cold-wet systems. Am Miner 101(5):1222–1227. https://doi.org/10.2138/am-2016-5591

Ludwig KR (2003) Isoplot 3.00: a geochronological toolkit for microsoft excel. Berkeley Geochronology Center Special Publication, Berkeley

Mattinson JM (2005) Zircon U-Pb chemical abrasion ("CA-TIMS") method: Combined annealing and multi-step partial dissolution analysis for improved precision and accuracy of zircon ages. Chem Geol 220:47–66. https://doi.org/10.1016/j.chemgeo.2005.03.011

McCurry M, Rodgers DW (2009) volume of mantle-derived magma. J Volcanol Geotherm Res 188:1–13. https://doi.org/10.1016/j.jvolgeores.2009.04.001

Morgan LA, McIntosh WC (2005) Timing and development of the Heise volcanic field, Snake River Plain, Idaho, western USA. Bull Geol Soc Am 117:288–306. https://doi.org/10.1130/B25519.1

Nash BP, Perkins ME, Christensen JN, Lee DC, Halliday AN (2006) The Yellowstone hotspot in space and time: Nd and Hf isotopes in silicic magmas. Earth Planet Sci Lett 247:143–156. https://doi.org/10.1016/j.epsl.2006.04.030

Pearce JA, Harris NBW, Tindle AG (1984) Trace element distribution diagrams for the tectonic interpretation of granitic rocks. J Petrol 25:956–983. https://doi.org/10.1093/petrology/25.4.956

Peng X, Humphreys ED (1998) Crustal velocity structure across the eastern Snake River Plain and the Yellowstone swell. J Geophys Res 103:7171–7186. https://doi.org/10.1029/97JB03615

Perkins ME, Brown FH, Nash WP, Williams SK, McIntosh W (1998) Sequence, age, and source of silicic fallout tuffs in middle to late Miocene basins of the northern Basin and Range province. Bull Geol Soc Am 110:344–360. https://doi.org/10.1130/0016-7606(1998)110<0344:SAASOS>2.3.CO;2

Pierce KL, Morgan LA (2009) Is the track of the Yellowstone hotspot driven by a deep mantle plume? - Review of volcanism, faulting, and uplift in light of new data. J Volcanol Geotherm Res 188:1–25. https://doi.org/10.1016/j.jvolgeores.2009.07.009

Rivera TA, Schmitz MD, Jicha BR, Crowley JL (2016) Zircon petrochronology and 40Ar/39Ar sanidine dates for the mesa falls tuff: Crystal-scale records of magmatic evolution and the short lifespan of a large yellowstone magma chamber. J Petrol 57:1677–1704. https://doi.org/10.1093/petrology/egw053

Ryan WBF, Carbotte SM, Coplan JO, O'Hara S, Melkonion A, Arko R, Weissel RA, Rerrini V, Woodwillie A, Nitsche F, Bonczkowski J (2009) Global multi-resolution topography synthesis. Geochem Geophys Geosyst 10:n/a–n/a. https://doi.org/10.1029/2008GC002332

Seligman AN (2012) Generation of low $\delta^{18}O$ silicic magmas, Bruneau-Jarbidge volcanic center, Yellowstone Hotspot: Evidence from zircons, including oxygen isotopes, U-Th-Pb dating, and melt inclusions. M.S. Thesis, University of Utah

Shervais JW, Evans JP, Schmitt DR, Christiansen EH, Prokopenko A (2014) Drilling into the track of the yellowstone hot spot. Eos (Washington DC) 95:85–86. https://doi.org/10.1002/2014EO100001

Shirley EK (2013). Precambrian history of cratonic North American crust beneath the Snake River Plain, Idaho; M.S. Thesis, Boise State University

Stelten ME, Cooper KM, Vazquez JA, Reid MR, Barfod GH, Wimpenny J, Yin QZ (2013) Magma mixing and the generation of isotopically juvenile silicic magma at Yellowstone caldera inferred from coupling 238U-230Th ages with trace elements and Hf and O isotopes in zircon and Pb isotopes in sanidine. Contrib Miner Pet 166:587–613. https://doi.org/10.1007/s00410-013-0893-2

Stelten ME, Cooper KM, Wimpenny JB, Vazquez JA, Yin QZ (2017) The role of mantle-derived magmas in the isotopic evolution of Yellowstone's magmatic system. Geochem Geophys Geosyst 18:1350–1365. https://doi.org/10.1002/2016GC006664

Szymanowski D, Ellis BS, Wotzlaw JF, Buret Y, von Quadt A, Peytcheva I, Bindeman IN, Bachmann O (2016) Geochronological and isotopic records of crustal storage and assimilation in the Wolverine Creek–Conant Creek system, Heise eruptive centre, Snake River Plain. Contrib Miner Pet 171:106. https://doi.org/10.1007/s00410-016-1314-0

Taylor HP, Forester RW (1979) An oxygen and hydrogen isotope study of the skaergaard intrusion and its country rocks: a description of a 55 Myr. old fossil hydrothermal system. J Petrol 20:355–419. https://doi.org/10.1093/petrology/20.3.355

Valley JW, Kitchen N, Kohn MJ, Niendorf CR, Spicuzza MJ (1995) UWG-2, a garnet standard for oxygen isotope ratios: Strategies for high precision and accuracy with laser heating. Geochim Cosmochim Acta 59:5223–5231. https://doi.org/10.1016/0016-7037(95)00386-X

von Quadt A, Wotzlaw J-F, Buret Y, Large SJE, Peytcheva I, Trinquier A (2016) High-precision zircon U/Pb geochronology by ID-TIMS using new 10^{13} ohm resistors. J Anal At Spectrom 31:658–665. https://doi.org/10.1039/C5JA00457H

Wang R, Tafti R, Hou ZQ, Shen ZC, Guo N, Evans NJ, Jeon H, Li QY, Li WK (2017a) Across-arc geochemical variation in the Jurassic magmatic zone, Southern Tibet: Implication for continental arc-related porphyry Cu[sbnd]Au mineralization. Chem Geol 451:116–134. https://doi.org/10.1016/j.chemgeo.2017.01.010

Wang W, Cawood PA, Zhou MF, Pandit MK, Xia XP, Zhao JH (2017b) Low-δ 18 O Rhyolites from the Malani Igneous Suite: a positive test for South China and NW India Linkage in Rodinia. Geophys Res Lett 44: 10,298–10,305. https://doi.org/10.1002/2017GL074717

Watts KE, Leeman WP, Bindeman IN, Larson PB (2010) Supereruptions of the Snake River Plain: two-stage derivation of low-$\delta^{18}O$ rhyolites from normal-$\delta^{18}O$ crust as constrained by Archean xenoliths. Geology 38:503–506. https://doi.org/10.1130/G30735.1

Watts KE, Bindeman IN, Schmitt AK (2011) Large-volume rhyolite genesis in caldera complexes of the Snake River Plain: insights from the Kilgore Tuff of the Heise volcanic field, Idaho, with comparison to Yellowstone and Bruneau-Jarbidge rhyolites. J Petrol 52:857–890. https://doi.org/10.1093/petrology/egr005

Wotzlaw JF, Schaltegger U, Frick DA, Dungan MA, Gerdes A, Günther D (2013) Tracking the evolution of large-volume silicic magma reservoirs from assembly to supereruption. Geology 41:867–870. https://doi.org/10.1130/G34366.1

Wotzlaw JF, Bindeman IN, Watts KE, Schmitt AK, Caricchi L, Schaltegger U (2014) Linking rapid magma reservoir assembly and eruption trigger mechanisms at evolved yellowstone-type supervolcanoes. Geology 42:807–810. https://doi.org/10.1130/G35979.1

Wotzlaw J-F, Bindeman IN, Stern RA, D'Abzac FX, Schaltegger U (2015) Rapid heterogeneous assembly of multiple magma reservoirs prior to Yellowstone supereruptions. Sci Rep 5:14026. https://doi.org/10.1038/srep14026

Wotzlaw J-F, Buret Y, Large SJE, Szymanowski D, von Quadt A (2017) ID-TIMS U-Pb geochronology at the 0.1‰ level using 1013 Ω resistors and simultaneous U and $^{18}O/^{16}O$ isotope ratio determination for accurate UO2 interference correction. J Anal At Spectrom 32:1–8. https://doi.org/10.1039/C6JA00278A

Zheng YF, Zhang SB, Zhao ZF, Wu YB, Li X, Li Z, Wu FY (2007) Contrasting zircon Hf and O isotopes in the two episodes of Neoproterozoic granitoids in South China: Implications for growth and reworking of continental crust. Lithos 96:127–150. https://doi.org/10.1016/j.lithos.2006.10.003

Zierenberg RA, Schiffman P, Barfod GH, Lesher CE, Marks NE, Lowenstern JB, Mortensen AK, Pope EC, Bird DK, Reed MH, Friðleifsson G, Elders WA (2013) Composition and origin of rhyolite melt intersected by drilling in the Krafla geothermal field, Iceland. Contrib Miner Pet 165:327–347. https://doi.org/10.1007/s00410-012-0811-z